

University of Louisville

ThinkIR: The University of Louisville's Institutional Repository

Electronic Theses and Dissertations

5-2014

Effect of metallic restoration artifacts on maxillofacial cone beam computed tomography images.

Mitali Binani 1987-
University of Louisville

Follow this and additional works at: <https://ir.library.louisville.edu/etd>



Part of the [Oral Biology and Oral Pathology Commons](#)

Recommended Citation

Binani, Mitali 1987-, "Effect of metallic restoration artifacts on maxillofacial cone beam computed tomography images." (2014). *Electronic Theses and Dissertations*. Paper 110.
<https://doi.org/10.18297/etd/110>

This Master's Thesis is brought to you for free and open access by ThinkIR: The University of Louisville's Institutional Repository. It has been accepted for inclusion in Electronic Theses and Dissertations by an authorized administrator of ThinkIR: The University of Louisville's Institutional Repository. This title appears here courtesy of the author, who has retained all other copyrights. For more information, please contact thinkir@louisville.edu.

EFFECT OF METALLIC RESTORATION ARTIFACTS ON MAXILLOFACIAL
CONE BEAM COMPUTED TOMOGRAPHY IMAGES

By

Mitali Binani

M.S, University of Louisville, 2014

A Thesis

Submitted to the Faculty of the School of Dentistry of the University of Louisville

In Partial Fulfillment of the Requirements

For the Degree of

Master of Science

Oral Biology

Louisville, Kentucky

May, 2014

EFFECT OF METALLIC RESTORATION ARTIFACTS ON MAXILLOFACIAL
CONE BEAM COMPUTED TOMOGRAPHY IMAGES.

By

Mitali Binani

M.S, University of Louisville, 2014

A Thesis Approved on

April 17, 2014

By the following Thesis Committee:

Dr. Allan G. Farman, Thesis Co-Director

Dr. William C. Scarfe, Thesis Co-Director

Dr. Bryan T. Harris, Committe Member

DEDICATION

This thesis is dedicated to my family and friends for their love and support. Without their encouragement, this thesis would not have been possible.

ACKNOWLEDGEMENTS

Dr. Allan G Farman, Thesis Co-Director, for providing me the opportunity to work under his guidance, and for contributing to this research project with his immense expertise in the specialty of Oral and Maxillofacial Radiology.

Dr. William C Scarfe, Thesis Co-Director, for his constant support and enthusiasm in all phases of the research. It was his relentless mentorship that made this project a successful endeavor.

Dr. Bryan T Harris, Thesis Committee Member, for his help to refine this project with his knowledge.

ABSTRACT

EFFECT OF METALLIC RESTORATION ARTIFACTS ON MAXILLOFACIAL CONE BEAM COMPUTED TOMOGRAPHY IMAGES.

Mitali Binani

April 17, 2014

Artifacts due to high-density objects (HDO) such as metallic dental restorations on maxillofacial cone beam computed tomographic (CBCT) images can render certain areas unsuitable for diagnosis. It was hypothesized that image quality due to HDO artifacts was affected by CBCT acquisition parameters and the number and configuration of HDO. Simulated complete maxillary and mandibular dental arches were constructed using dental stone and extracted teeth. Conservative coronal dental amalgam (MOD) restorations on premolar and molar teeth were used as HDOs. Gray values (GV) measured on uniform dental stone test cylinders at specific levels from the occlusal plane at three tooth locations was used as an index of artifact effect on image quality. Scans with various HDO configurations were taken at several acquisition parameters for three CBCT systems: Accuitomo 170 (J. Morita MFG. Corp, Kyoto, Japan), iCAT Next Generation (Imaging Sciences International Inc., Hatfield, PA, USA) and Carestream 9000 3D (Carestream/KODAK, Atlanta, GA). For all systems, HDOs significantly affected images throughout the field of view, with machine specific beam hardening or scatter artifacts. Worst beam hardening affected areas were within 0mm-4mm of the occlusal plane of the ipsilateral test cylinder. The Accuitomo 170 was unaffected by

acquisition parameters. Caution must be exercised when assessing CBCT images for coronal dental caries and other pathologies in the presence of HDOs to prevent errors in diagnosis due to beam hardening or scatter artifacts.

TABLE OF CONTENTS

	<i>PAGE</i>
DEDICATION	iii
ACKNOWLEDGMENTS	iv
ABSTRACT	v
LIST OF FIGURES	ix
LIST OF TABLES	x
INTRODUCTION AND LITERATURE REVIEW	1
HYPOTHESIS	5
Objectives	5
Null Hypothesis	6
MATERIALS AND METHODS	7
Overall Research Design	7
In vitro model	8
High Density Object (HDO) Configuration	10
Cone Beam Computed Tomographic Imaging	10
Analysis	14
CBCT Image Evaluation	14
Data Analysis	14
RESULTS	16
Overview	16
Descriptive	17
Analytical	25
DISCUSSION	49
CONCLUSION	53

REFERENCES.....	54
APPENDIX A.....	56
CURRICULUM VITAE.....	60

LIST OF FIGURES

<i>FIGURE</i>	<i>PAGE</i>
1. CS 9000 interval plot showing Δ GV% for each test cylinder location according to each independent variable (Depth, kV and resolution)	19
2. CS 9000 interval plot of Δ GV% (y-axis) according to position of the HDO relative to the test cylinder (adjacent vs. non-adjacent) for the CS 9000D	20
3. iCAT NG interval plot showing Δ GV% for each test cylinder location according to each independent variable (Depth, kV and resolution).	21
4. iCAT NG interval plot showing Δ GV% for each test cylinder location according to each independent variable (Depth, kV and resolution) according to position of the HDO relative to the test cylinder (adjacent vs. non-adjacent).	22
5. 3D Accuitomo 170 interval plot showing Δ GV% for each test cylinder location according to each independent variable (Depth, kV and resolution).	23
6. 3D Accuitomo 170 interval plot showing Δ GV% for each test cylinder location according to each independent variable (Depth, kV and resolution) according to position of the HDO relative to the test cylinder (adjacent vs. non-adjacent).	24

LIST OF TABLES

<i>TABLE</i>	<i>PAGE</i>
1. Summary of Studies on the Diagnostic Accuracy of CBCT in the Detection of Dental Caries	2
2. Comparison of gray values of dentin in the control model (without HDO) and patient radiographs (without HDO) on iCAT Next Generation CBCT Unit (120 kV / 5 mA).....	9
3. Gray values of dentin on control model on Accuitomo 170 and Carestream 9000 3D	9
4. Location of High Density Objects	11
5. Exposure parameters for the Carestream 9000 3D CBCT System	12
6. Exposure parameters for the iCAT Next Generation CBCT System	12
7. Exposure parameters for the Acciutomo 170 CBCT System.....	13
8. Choosing the Appropriate Multiple Comparison Test - Normality (Anderson-Darling test) And Equal Variance Tests for independent variables for each CBCT unit	18
9. CS 90003D GLM.....	25
10. <i>Post Hoc</i> pairwise comparison (Tukey) for Δ GV% for various configurations of HDO Artifact	27
11. <i>Post Hoc</i> pairwise comparison (Tukey) for Δ GV% at various level of cylinder ..	30
12. <i>Post Hoc</i> pairwise comparison (Tukey) for Δ GV% at various arch locations	31
13. <i>Post Hoc</i> pairwise comparison (Tukey) for Δ GV% at two kV levels.	31
14. <i>Post Hoc</i> pairwise comparison (Tukey) for Δ GV% at high and low resolutions ..	31
15. <i>Post Hoc</i> pairwise comparison (Tukey) for Δ GV% according to the side where HDO is positioned.	32

16. <i>Post Hoc</i> pairwise comparison (Tukey) for Δ GV% at position of HDMO relative to test cylinder	32
17. Analysis of Variance for iCAT Next Generation	33
18. <i>Post Hoc</i> pairwise comparison (Tukey) for Δ GV% for various configurations of HDOs	35
19. <i>Post Hoc</i> pairwise comparison (Tukey) for Δ GV% at various level of cylinder ..	38
20. <i>Post Hoc</i> pairwise comparison (Tukey) for Δ GV% at various arch locations	39
21. <i>Post Hoc</i> pairwise comparison (Tukey) for Δ GV% at two resolutions.	39
22. <i>Post Hoc</i> pairwise comparison (Tukey) for Δ GV% at two arches	39
23. <i>Post Hoc</i> pairwise comparison (Tukey) for Δ GV% according to side of HDO....	40
24. <i>Post Hoc</i> pairwise comparison (Tukey) for Δ GV% according to proximity of HDMO to test cylinder.....	40
25. 3D Accuitomo 170 Analysis of Variance	41
26. <i>Post Hoc</i> pairwise comparison (Tukey) for Δ GV% for various configurations of artifacts.....	43
27. <i>Post Hoc</i> pairwise comparison (Tukey) for Δ GV% at various levels of cylinder.	46
28. <i>Post Hoc</i> pairwise comparison (Tukey) for Δ GV% at various arch locations	47
29. <i>Post Hoc</i> pairwise comparison (Tukey) for Δ GV% at two arches	47
30. <i>Post Hoc</i> pairwise comparison (Tukey) for Δ GV% according to side of HDO in the arch.....	48
31. <i>Post Hoc</i> pairwise comparison (Tukey) for Δ GV% according to proximity of HDO to test cylinder	48

CHAPTER I

INTRODUCTION AND LITERATURE REVIEW

Maxillofacial cone beam computed tomography (CBCT) has helped improve diagnosis, treatment planning and follow up with much more accurate and precise imaging. However, there are still some inherent artifacts produced that limit the use of this technology for specific tasks. These introduce errors that reduce image quality and should be considered with clinical use.

The most common patient related artifacts produced in the field of view (FOV) of CBCT are as a result of the presence of high-density objects (HDO) such as amalgam, composite resin, implants, etc. Attenuation and interaction of x-rays with HDO produce scatter, beam hardening, and photon starvation and produce images with dark and light streak artifacts.⁽¹⁾ These artifacts are more intense in the mesio-distal region of the HDO^(2, 3) and may be severe enough so as to render the scans unsuitable for interpretation. In a retrospective, observational study, Ritter, *et al.*⁽⁴⁾ concluded that restorations negatively impact the image quality of CBCT images. They specifically used the Galileos CBCT system (Sirona Dental Systems, Bensheim, Germany). Since much of the population have dental amalgam restorations, it is important to quantitatively assess the effect of the presence of dental amalgam with the pattern and intensity of artifacts produced and ultimately correlate this with the diagnostic yield of CBCT specifically for the assessment of coronal conditions such as the detection of the presence of dental caries.

There is significant controversy regarding the assertion that CBCT is potentially a better diagnostic imaging tool for coronal dental caries than conventional radiography (Table 1).

Table 1. Summary of Studies on the Diagnostic Accuracy of CBCT in the Detection of Dental Caries

<i>Author reference</i>	<i>Year</i>	<i>Caries</i>		<i>Modality</i>		<i>Results</i>
		<i>Type of teeth</i>	<i>Surface</i>	<i>CBCT</i>	<i>Intraoral</i>	
		<i>D / P</i>	<i>Occ / Prox</i>			
(5)	2006	P	Prox	Limited cone beam computed tomography (LCBCT)	Image plate system and F-speed film	LCBT fared better than intra oral radiography in detecting proximal caries.
(6)	2007	P	Prox	3D Accuitomo (J. Morita Mfg. Corp., Kyoto, Japan)	Insight films (Eastman Kodak, Rochester, NY)	No difference between accuracy in detecting proximal carious lesion
(7)	2008	P	Both	NewTom 3G and 3DX Accuitomo	Digora-fmx and Kodak Insight films	NewTom 3G has lower diagnostic accuracy than others.
(8)	2008	CBCT systems are better than intraoral systems at detecting carious lesions when no metallic elements present in the oral cavity.				
(9)	2009	P	Both	3DX Accuitomo	Gendex 1000 X-ray unit	3DX high resolution CBCT fare better in detecting proximal caries but not occlusal caries when compared with CCD images.
(10)	2010	P	Prox	ILUMA ultra cone beam CT scanner	Trophy Trex X-ray unit, Progeny Vision DX, Digora Optime,	No significant difference between the systems.

Table 1(Continued). Summary of Studies on the Diagnostic Accuracy of CBCT in the Detection of Dental Caries

<i>Author reference</i>	<i>Year</i>	<i>Caries</i>		<i>Modality</i>		<i>Results</i>
		<i>Type of teeth</i>	<i>Surface</i>	<i>CBCT</i>	<i>Intraoral</i>	
(11)	2011	P	Prox	NewTom 9000; Accuitomo 3DX; Kodak 9000 3D; ProMax 3D; and DCT PRO		No significant difference between systems.
(12)	2011	P	Both	Kodak 9500 Cone Beam 3D System	Trophy ETX intraoral X-ray unit and Digora Optime	Significant difference seen between CBCT and conventional radiography for occlusal caries. No significant difference between systems for proximal caries.
(13)	2011	P	Prox	Pax-500ECT, ProMax 3D	F-speed films (Insight Dental Film)	CBCT fared better than intraoral radiography in detecting secondary caries.
(14)	2013	P	Prox	3D Accuitomo FPD80	Digora Toto Digora Optime	CBCT fared better than intraoral systems in detecting approximal carious lesions
(15)	2014	P	Prox	Kodak 9000 3D		CBCT was more accurate in detecting cavitation in proximal surfaces than bitewing radiographs

D, deciduous; P, permanent; Occ, occlusal; Prox, proximal; VI, visual inspection; F; analog film; CCD, charged coupled device; PSP, photostimulable storage phosphor

Many authors ^(6, 10-12) have indicated that CBCT systems offer no significant improvement on the diagnosis of dental caries when compared with intraoral radiographic techniques. However, some authors ^(5, 9, 14, 15) have reported greater caries detection using CBCT systems than intraoral radiography. Only Charuakkra, *et al.*, ⁽¹³⁾ reported CBCT to be better than film-based bitewing techniques at diagnosing artificially created, secondary caries under proximal, radiopaque restorations. No studies in the current literature have explored the potentially deleterious effect of HDO, particularly coronal metallic dental restorations, on dental caries diagnosis.

Extensive review of the English literature indicates that no author has yet quantified the effect of artifact production by coronal HDO (e.g. dental amalgam) in CBCT images. The purpose of this investigation is to help characterize image quality degradation of beam hardening and scatter introduced on adjacent and regional dental tooth structures when HDOs are introduced into CBCT images. This should provide a theoretical basis for further studies on the effect of HDO's on the detection of coronal dental caries diagnosis on CBCT images with the presence of dental amalgam in the dental arch.

CHAPTER II

HYPOTHESES

Objectives

The aims of this research are:

- To develop an *in vitro* anatomic model representative of the human dental arches incorporating extracted human teeth with bone and soft tissue simulation material corresponding to human voxel gray values (GV) on images.
- To develop a sequence of HDO configurations within the *in vitro* model of the dental arches representing increasing local and overall artifact effects to simulate various clinical scenarios.
- To quantify the effect of artifacts on local and peripheral noise on axial images obtained on 3 different CBCT systems by measuring the variability of gray value (GV) on homogeneous test cylinders acting as controls at standard positions using a non-proprietary, readily available medical/dental image software program.
- To quantify the effect of the following independent variables on the local and peripheral noise (dependent variable) on images obtained on 3 different CBCT systems:
 - Inter-arch position (Maxilla/Mandible)
 - Number of HDO

- Intra-arch position (Location of HDO relative to controls)
- Variations in acquisition settings (kV, nominal resolution, exposure time and number of basis images)

Null Hypothesis

It is hypothesized that:

- There are no effects on image quality on CBCT images with the introduction of HDO (i.e. dental amalgam).
- The effects on image quality on CBCT images with the introduction of HDO does not depend upon the inter-arch position (Maxilla/Mandible) of HDOs.
- The effects on image quality on CBCT images with the introduction of HDO does not depend upon intra-arch number of HDOs.
- The effects on image quality on CBCT images with the introduction of HDO does not depend upon intra-arch proximity (unilateral, anterior or contralateral) of HDOs.
- The effects on image quality on CBCT images with the introduction of HDO does not depend upon CBCT acquisition parameters such as kV, nominal resolution, exposure time and number of basis projections.

CHAPTER III

MATERIALS AND METHODS

Overall Research Design:

This *in vitro* laboratory-based study was designed to provide a quantitative analysis of the effects of CBCT image artifacts produced by high density objects (HDOs) such as metallic restorations on image quality using a simulated model of the dental arches imaged at various acquisition parameters with three (3) CBCT systems. Image quality was measured as the percentage difference between gray values ($\Delta GV\%$) on a fiducial test cylinder of homogeneous radiodensity in a control and treatment phantom. Fiducial cylinders were positioned at three representative tooth sites (right second premolar, central incisor, and left second premolar) within the dental arches (maxilla/mandible) with fifteen (15) configurations of HDOs using three (3) CBCT units operated at several exposure parameters:

1. 3D Accuitomo 170; J Morita MFG. Corp, Kyoto, Japan (Accuitomo 170)
2. iCAT Next generation; iCAT model 17-19, Imaging Sciences International Inc., Hatfield, PA, USA. (iCAT NG)
3. Carestream 9000 3D, Carestream/KODAK, Atlanta, GA. (CS 9000)

In vitro Simulated Dental Arch Model

Maxillary and mandibular dental arch models were fabricated to simulate the dentition aligned in the average human dental arch form. Initially a life size template was created based on the average shape of human dental arches⁽¹⁶⁾ using utility wax. An impression of the wax models was then taken using alginate (Jeltrate, Dentsply Caulk, Milford, Del.). During pour with type III dental stone (Quickstone, Whip Mix Corporation, Louisville, KY, USA), utility wax was inserted as a substitute for alveolar bone proper to enable insertion of extracted teeth within the reproduced dental arches. Dental stone mixed with plastic round pellets (Freeplastic, Daicel Craft Ltd., Tokyo) simulated the radio density of bone⁽²⁾ and bone marrow in the jaws respectively. Permanent, non-carious, unrestored, sterilized, extracted teeth were used to construct a maxillary and mandibular dental arch. Three uniform test cylinders (average size of a premolar; 25mm [height] x 5mm [diameter]) made of type V jade stone (Whip Mix Corporation Louisville, KY, USA) replaced the right central incisor, right and left second premolars in each dental arch. These provided control fiducial objects at three locations with uniform, homogeneously dense material with mean density gray values (GV) approximating dentin. Water was mixed with jade stone in the ratio of 15.5ml/70g to achieve a radiodensity similar to that of dentin as measured on a subset of CBCT patient scans (iCAT NG) with no HDOs (Table 2). Measurements were obtained by exporting the DICOM (Digital Image and Communication in Medicine) data and importing it into a non-proprietary image analysis software (OSIRIX MD; Osirix Foundation, Geneva, Switzerland). Gray values of dentin in the same locations as in Table 2, for control models, scanned by Accuitomo 170 and Carestream 9000 3D are given in Table 3.

Table 2. Comparison of gray values of dentin in the control model (without HDO) and patient radiographs (without HDO) on iCAT Next Generation CBCT Unit (120 kV / 5 mA).

<i>Patient</i>	<i>Age (yrs)</i>	<i>Res</i>	<i>No. of basis images</i>	<i>Maxillary</i>				<i>Mandibular</i>			
				<i>PM1</i>		<i>M1</i>		<i>PM1</i>		<i>M1</i>	
				<i>R</i>	<i>L</i>	<i>R</i>	<i>L</i>	<i>R</i>	<i>L</i>	<i>R</i>	<i>L</i>
Control		0.4	200	986	1076	1117	1118	1220	1196	1029	1009
Control		0.25	325	970	1026	871	968	1135	1169	966	969
1	20	0.3	576	878	878	779	835	827	985	707	993
2	16	0.3	576	930	965	1037	907	857	990	1075	879
3	14	0.3	576	1740	1798	1658	1793	1553	1482	1658	1573
4	16	0.3	576	1015	940	1131	1058	1158	874	1181	958
5	19	0.3	576	866	908	787	775	739	881	827	833
MEAN GV for Patients				1085	1038	1053	1056	1124	1057	1026	1040

**Res, resolution; PM1, First Premolar; M1, First Molar.*

Table 3. Gray values of dentin on control model on Accuitomo 170 and Carestream 9000 3D.

<i>Patient</i>	<i>CBCT</i>	<i>kV</i>	<i>mAs</i>	<i>Res</i>	<i>No. of basis images</i>	<i>Maxillary</i>				<i>Mandibular</i>			
						<i>PM1</i>		<i>M1</i>		<i>PM1</i>		<i>M1</i>	
						<i>R</i>	<i>L</i>	<i>R</i>	<i>L</i>	<i>R</i>	<i>L</i>	<i>R</i>	<i>L</i>
Control	Acc	90	5	0.25	1008	1497	1381	1487	1457	1384	1555	1397	1384
	Acc	75	5	0.25	1007	1524	1376	1332	1226	1597	1602	1323	1276
	Acc	90	5	0.25	584	1254	1439	1258	1279	1377	1408	1542	1439
	Acc	75	5	0.25	584	1567	1731	1526	1531	1611	1619	1775	1758
	CS 3D	90	10	0.2	360	1357	1536	1308	1495	1432	1573	1394	1326
	CS 3D	75	10	0.2	360	1408	1429	1468	1424	1465	1579	1379	1310
	CS 3D	90	10	0.08	360	1451	1580	1470	1667	1210	1260	1323	1477
	CS 3D	75	10	0.08	360	1385	1454	1301	1616	1311	1305	1468	1304

**Res, resolution; PM1, First Premolar; M1, First Molar.*

The models were imaged multiple times at various exposure parameters with removal and substitution of specific teeth with comparable teeth prepared with standard, mesial-occlusal-distal (MOD) dental amalgam coronally restored premolars and molars. Insertion of the restored teeth was performed in a specific configuration representing an increasing level of coronal high density objects (HDO). The entire model was immersed in water to simulate soft tissue attenuation within the head. After many samples were tried, the most appropriate container [8" (height) x 6.5" (diameter) with water filled at the 4.5" mark], which fit the model and could hold enough water to simulate attenuation within the head, was used. Images of the dental arches with unrestored teeth without coronal HDO at each exposure parameter were used as controls.

High Density Object (HDO) Configuration

Dental amalgam restored teeth were arranged in fifteen (15) configurations to reproduce imaging scenarios of increasing unilateral and bilateral coronal HDO in the dental arches (Table: 4) (Appendix A).

Cone Beam Computed Tomographic Imaging

Three (3) CBCT systems were used to image the maxillary and mandibular models together. For each system, the dental arch models with no HDOs present were imaged at each exposure setting (control). Then the models with HDOs according to the fifteen (15) configurations previously described (six unilateral and nine bilateral) were imaged. The total number of scans performed for each unit was equal to the number of exposure settings used (y) times the HDO configurations used (15).

Table 4. Location of High Density Objects

<i>Config.</i>	<i>Relative to the Dental Arch</i>	<i>Relative to the Test Cylinder</i>	<i>Specific Configuration of HDO</i>	
			<i>Right</i>	<i>Left</i>
1	Unilateral	Adjacent to test cylinder	PM1	-
5			M1 & M2	-
9			M1 & M2 & M3	-
2	Unilateral	One tooth away from test cylinder	M2	-
6			M2 & M3	-
3	Unilateral	Two teeth away from test cylinder	M3	-
12	Bilateral	Adjacent to test cylinder	PM1	PM1
15			M1	M1 & M2
16			M1	M1, M2 & M3
18			M1 & M2	M1 & M2
19			M1 & M2	M1, M2 & M3
21			M1, M2 & M3	M1, M2 & M3
13	Bilateral	One tooth away from test cylinder	M2	M2
24			M2 & M3	M2 & M3
25	Bilateral	Two teeth away from test cylinder	M3	M3

Config.: Configuration; PM1: First Premolar; M1: First Molar; M2: Second Molar; M3: Third Molar

1) Carestream 9000 3D

The exposure parameters used with the Carestream 9000 3D (Carestream Health, Atlanta, GA) CBCT unit are shown in Table 4. The model was attached on the base provided by the manufacturer and oriented in the center of FOV, with the occlusal plane parallel to the horizontal plane using laser orientation beams. As this CBCT system has a limited FOV, images were taken separately for three regions (Anterior, left and right posterior) at the exposure parameters shown in Table 5. Axial slices at the default nominal resolution were exported as uncompressed, multi-file images in DICOM format from the proprietary software (KODAK Dental Imaging Software 6.11.7.0, Carestream

Health Inc.,2007, Atlanta, GA) and imported into OsiriX MD software (OsiriX Foundation, Geneva, Switzerland) for analysis.

Table 5. Exposure parameters for the Carestream 9000 3D CBCT System

<i>kV</i>	<i>mA</i>	<i>Nominal Resolution (mm)</i>	<i>Mode</i>	<i>Time (s)</i>	<i>FOV (diameter x height)(cm)</i>
90	10	0.2	-	10.62*	5*3.7
90	10	0.076	-	10.59^	5*3.7
75	10	0.2	-	10.62	5*3.7
75	10	0.076	-	10.62	5*3.7

*360 basis images

2) iCAT Next Generation System

The exposure parameters used with the iCAT (Next Generation, Imaging Sciences International, Hatsfield, PA) are shown in Table 6. The model was placed on the base provided by the manufacturer, in the center of FOV and aligned with the horizontal plane using the laser light system for orientation. Scout images were taken prior to scanning to ensure correct placement of the model. Axial slices at the default nominal resolution were exported as uncompressed, multi-file images in DICOM format from the proprietary software (i-CATVision Q™ software (Imaging Sciences International, Hatsfield, PA) and imported into OsiriX MD software for analysis.

Table 6. Exposure parameters for the iCAT Next Generation CBCT System

<i>kV</i>	<i>mA</i>	<i>Nominal Resolution (mm)</i>	<i>Mode</i>	<i>Time (s)</i>	<i>FOV (diameter x height) (cm)</i>
120	5	0.4	-	4.8*	160*80
120	5	0.25	-	26.9^	160*80

*160 Basis images; ^ 619 Basis images

3) Accuitomo 170

The exposure parameters used with the 3D Accuitomo 170 (J. Morita, Kyoto, Japan) CBCT system is shown in Table 7. Using boxes as support, models were elevated to enable alignment within the field of view (FOV) using the laser positioning lights such that the occlusal plane was parallel to the horizontal plane and models were in the center of the field of view (FOV). Scout images were taken to confirm the correct positioning of the model within the FOV. Default 0.25mm axial images were exported as uncompressed multi-file images in Digital Imaging and Communications in Medicine (DICOM) format from the proprietary software (iDixel image processing software, J. Morita USA, Inc, Irvine, USA) and imported into OsiriX MD software for analysis.

Table 7. Exposure parameters for the Accuitomo 170 CBCT System

<i>kV</i>	<i>mA</i>	<i>Nominal Resolution (mm)</i>	<i>Mode</i>	<i>Time (s)</i>	<i>FOV (diameter x height) (cm)</i>
90	5	0.25	Standard*	17.5	140*100
90	5	0.25	Hi-fi [^]	30.8	140*100
75	5	0.25	Standard*	17.5	140*100
75	5	0.25	Hi-fi [#]	30.8	140*100

**584 Basis images; [^]1008 Basis images; [#]1007 Basis images*

Analysis

CBCT Image Evaluation

All images were imported into OsiriX MD (OsiriX Foundation, Geneva, Switzerland) to avoid any disparity in measurements produced by using unit specific proprietary CBCT system softwares. Osirix MD was chosen for this evaluation because, unlike other softwares that were tried, this software was able to uncompress and open DICOM files from all the CBCT systems that were used.

X-ray attenuation, in terms of mean grey value (GV), was measured at six levels relative to the occlusal plane vertically on each test cylinder: at the occlusal plane (0mm), 2mm, 4mm, 10mm, 15mm, and 25mm. The level on each cylinder was measured from the occlusal surface of amalgam restorations. To facilitate reproducibility, the density region of interest (ROI) was customized and fixed at 0.175 cm^2 and used for every measurement. A square of an area of 0.175 cm^2 was found to be the largest area that fit within the circumference of the test cylinder. The same protocol was used for all experimental and control models.

Data Analysis

Benic, *et al.*,⁽²⁾ used a methodology to study the effect of beam hardening around implants by comparing mean GV values circumferentially around implants. This methodology was adapted for use in this research. Mean GV measured within the defined ROI on control models for each scanning parameter was designated as GV_{control} . Differences of gray values (ΔGV) between models with (GV_{Test}) and without (GV_{control}) HDO were calculated as percentages using the following formula:

$$\Delta GV\% = [(GV_{Test} - GV_{control})/GV_{control}] * 100.^{(2)}$$

Graphically, mean GV% was plotted overall for each test cylinder (ipsilateral, center, contralateral) and again according to adjacent and non-adjacent groups of configurations against the independent variables. Each CBCT system has its own confounding variables that make statistical comparison between the systems, using the results from this experimental method, biased. Therefore for each CBCT system, the GV% values were analyzed statistically by the General Linear model by comparing mean values in a MANOVA design against all independent variables with HDO present unilaterally and bilaterally (Table 4) and at different parameters (Table 5,6,7) on the same CBCT system.

CHAPTER IV

RESULTS

Overview

Two approaches were used to analyze and present the data:

- 1) To visualize and describe trends for each CBCT unit, descriptive statistics were provided by plotting two graphs:
 - a. An overall graph of $\Delta GV\%$ (y-axis) for each test cylinder location (Center, contralateral and, ipsilateral) according to each independent variable and,
 - b. A second graph stratifying these results according to position of the HDO relative to the test cylinder (adjacent vs. non-adjacent).
 - 2) Statistical comparison to compare the effects of the categorized independent variables. The multiple categorical analysis for parametric data is ANOVA. However, application of ANOVA assumes that the data conforms to two assumptions:
 - a. The data is normally distributed (Poisson distribution), and
 - b. They data have equal variances (Ranges / s.d. are similar).
- Prior to performing the analysis, grouped independent variables were analyzed to determine Normality (Anderson-Darling test for Normality) and Equal variances (F-test for normally distributed data and Levene's Test for non-normally distributed data). Because overall the data for $\Delta GV\%$ were not normally

distributed nor had equal variances (Table 8), the general linear model was chosen.

1) Descriptive

For each CBCT unit two plots are generated. The assumptions are that $\Delta GV\%$ is an index of image quality. Interpretation of the values for $\Delta GV\%$ was as follows:

- A $\Delta GV\%$ close to zero (0) means that there is little or no difference in image quality between the phantom with no HDOs (control) and the phantom with HDOs (test).
- A $-\Delta GV\%$ depicts a relative hyper-density or dark region associated with beam hardening and,
- A $+\Delta GV\%$ is a relative hypo-density or light region associated with scattered radiation.

The first figure shows the overall plot of $\Delta GV\%$ (y-axis) for each test cylinder location (center, contralateral and, ipsilateral) according to each independent variable. The second plot shows the plot of $\Delta GV\%$ (y-axis) according to position of the HDO relative to the test cylinder (adjacent vs. non-adjacent).

Table 8. Choosing the Appropriate Multiple Comparison Test - Normality (Anderson-Darling test) And Equal Variance Tests for independent variables for each CBCT unit

<i>CBCT Unit</i>	<i>Independent Variable</i>	<i>Normality</i>			<i>Equal Variances*</i>			
		<i>A</i>	<i>N</i>	<i>Sig.</i>	<i>Bartlett t's Test</i>	<i>Sig. †</i>	<i>Levene's Test</i>	<i>Sig. †</i>
CS 9000		11.039	2160	<0.005				
	Config.				201.45	0.000	8.92	0.000
	Depth				308.33	0.000	45.05	0.000
	Arch				0.94	0.288	0.07	0.798
	Location				133.53	0.000	37.44	0.000
	kV				1.04	0.514	0.78	0.376
	Resolution				2.20	0.000	76.27	0.000
	Sidedness				2.19	0.000	104.64	0.000
	Proximity				1.30	0.000	8.69	0.003
iCAT NG		180.70	1080	<0.005				
	Config.				3024.8	0.000	38.11	0.000
	Depth				20.93	0.001	1.90	0.091
	Arch				1.32	0.001	1.83	0.176
	Location				14.51	0.001	2.69	0.069
	Resolution				0.84	0.049	0.52	0.471
	Sidedness				372.10	0.000	295.05	0.000
	Proximity				307.07	0.000	282.77	0.000
Accutom o 170		498.74	2160	<0.005				
	Config.				4695.1	0.000	85.58	0.000
	Depth				71.09	0.000	1.44	0.206
	Arch				1.42	0.000	5.53	0.019
	Location				60.54	0.000	5.45	0.004
	kV				0.78	0.000	0.53	0.466
	Frames				1.03	0.628	0.12	0.732
	Sidedness				33.15	0.000	231.30	0.000
	Proximity				46.88	0.000	229.33	0.000

Sig., statistical significance; Config., Configuration

** The use of F-Test or Levene's Test depends on the normality of the data. If the data is normally distributed then the F-Value should be used. If the data is not normally distributed then the Levene's test should be used.*

† If $p > 0.05$, the variances can be assumed to be roughly the same and ANOVA assumptions are valid.

CS 9000

Figure 1. CS 9000 interval plot showing Δ GV% for each test cylinder location according to each independent variable (Depth, kV and resolution)

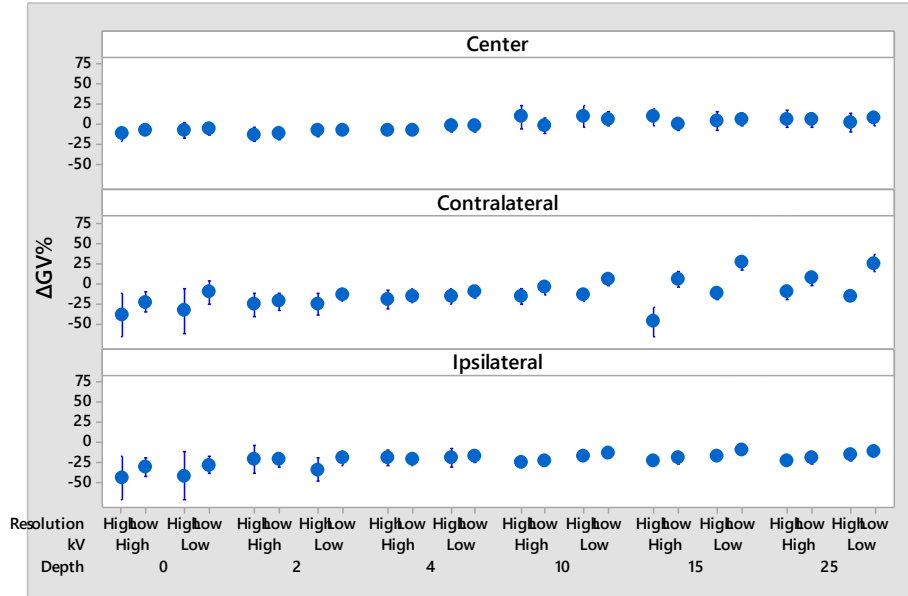


Figure 1 shows the overall plot of Δ GV% (y-axis) for the CS 9000D. As a trend, overall image quality (Δ GV%):

- Is reduced overall due to the effects of HDO by increasing the overall density of the image due to beam hardening ($-\Delta$ GV%),
- Is worse for ipsilateral cylinders followed by contralateral followed by anteriorly placed cylinders,
- Is better with lower resolution (0.2mm) than higher resolution (0.076mm) particularly for contralateral and ipsilateral cylinders,
- Appears to be independent of kV,
- Improves with increasing distance from the occlusal plane, especially within 2mm to 4mm.
- Appears to be independent of arch (maxillary/mandibular).

Figure 2. CS 9000 interval plot showing $\Delta\text{GV}\%$ for each test cylinder location according to each independent variable (Depth, kV and resolution) according to position of the HDO relative to the test cylinder (adjacent vs. non-adjacent).

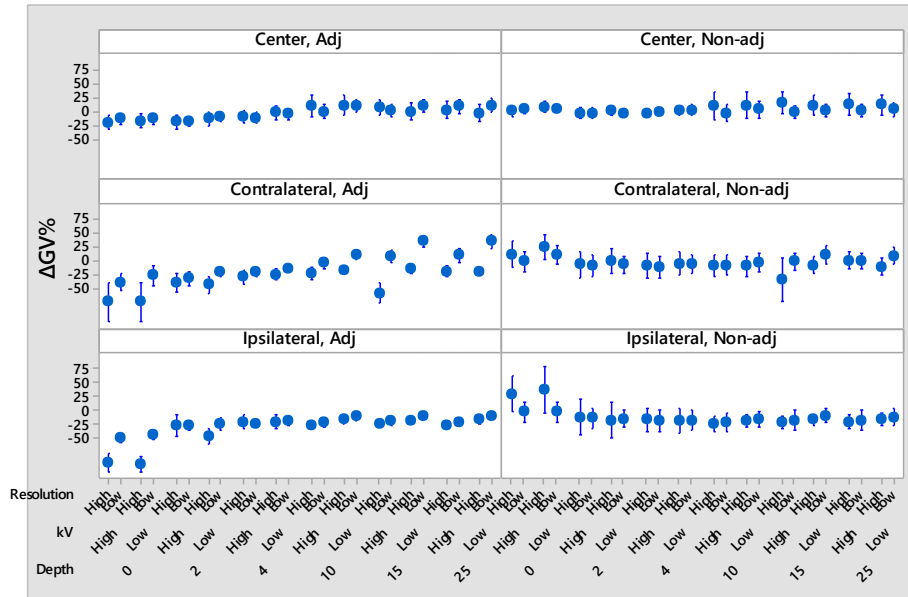


Figure 2 shows a plot of $\Delta\text{GV}\%$ (y-axis) according to position of the HDO relative to the test cylinder (adjacent vs. non-adjacent) for the CS 9000D. As a trend, image quality ($\Delta\text{GV}\%$):

- Is independent of the position of the HDO in the anterior region.
- Is worse on both the ipsilateral and contralateral side when the HDO is adjacent the test cylinder,
- Is worse for high resolution than low resolution for both contralateral and ipsilateral sides when the HDO is adjacent to the cylinder,
- Beam hardening effects are reduced ($-\Delta\text{GV}\%$) and scattering effects become more prominent ($\Delta\text{GV}\%$ becomes more positive) for both contralateral and ipsilateral sides when the HDO is non-adjacent to the cylinders; this appears to be more pronounced for high resolution than low resolution,
- Appears to be independent of kV, irrespective of position of the HDO,

- Improves with increasing distance from the occlusal plane, with the greatest change occurring from 2mm to 4mm.

iCAT Next Generation

Figure 3. iCAT NG interval plot showing Δ GV% for each test cylinder location according to each independent variable (Depth, kV and resolution).

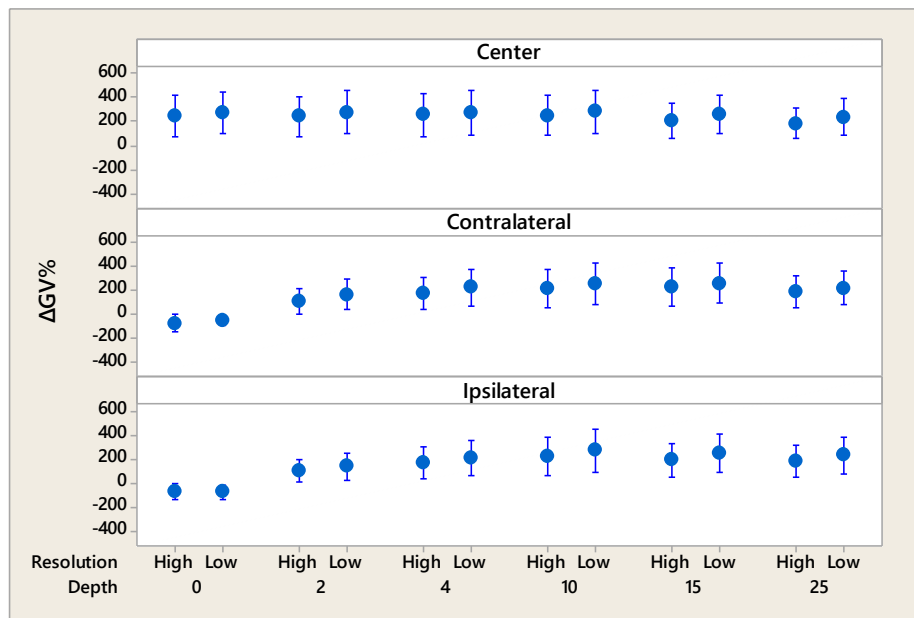


Figure 3 shows the overall plot of Δ GV% (y-axis) for the iCAT NG. As a trend, overall image quality (Δ GV%):

- Is reduced due to scatter (+ Δ GV%) for anterior cylinders similarly at all heights relative to the occlusal plane,
- Is reduced due to beam hardening (- Δ GV%) at the level of the occlusal plane for both ipsilateral and contralateral cylinders,
- Is reduced due to scatter is (+ Δ GV%) at levels below the occlusal plane for both ipsilateral and contralateral cylinders reaching a plateau at about 10mm,
- Is reduced with lower resolution (0.2mm) than higher resolution (0.076mm),

particularly for contralateral and ipsilateral cylinders.

Figure 4. iCAT NG interval plot showing $\Delta\text{GV}\%$ for each test cylinder location according to each independent variable (Depth, kV and resolution) according to position of the HDO relative to the test cylinder (adjacent vs. non-adjacent).

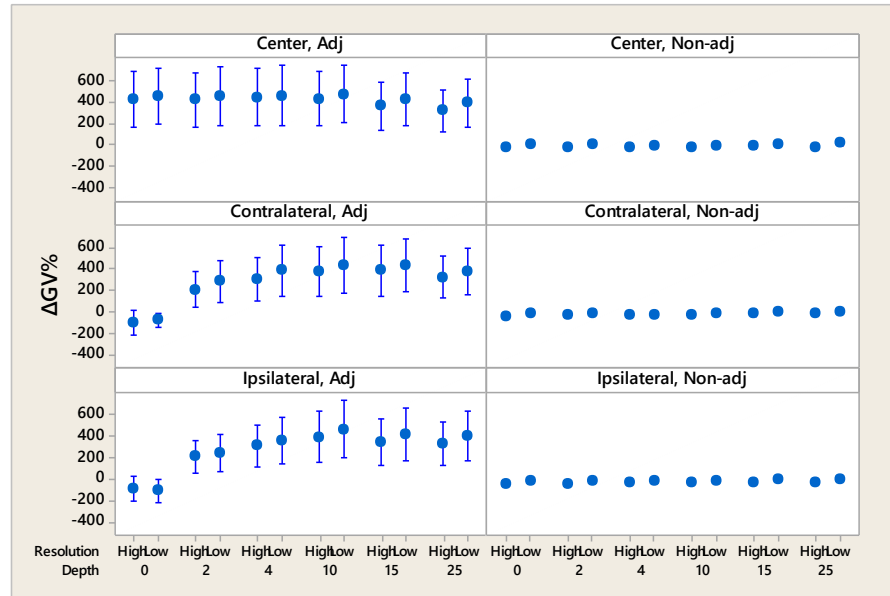


Figure 4 shows a plot of $\Delta\text{GV}\%$ (y-axis) according to position of the HDO relative to the test cylinder (adjacent vs. non-adjacent) for the iCAT NG. As a trend, image quality ($\Delta\text{GV}\%$):

- Is minimally affected or marginally reduced due to beam hardening ($-\Delta\text{GV}\%$) when HDOs are non-adjacent to the test cylinder at all positions (center, contr- and ipsilateral),
- Follows similar trends as described above when HDOs are adjacent the test cylinder.

3D Accuitomo 170

Figure 5. 3D Accuitomo 170 interval plot showing $\Delta\text{GV}\%$ for each test cylinder location according to each independent variable (Depth, kV and resolution).

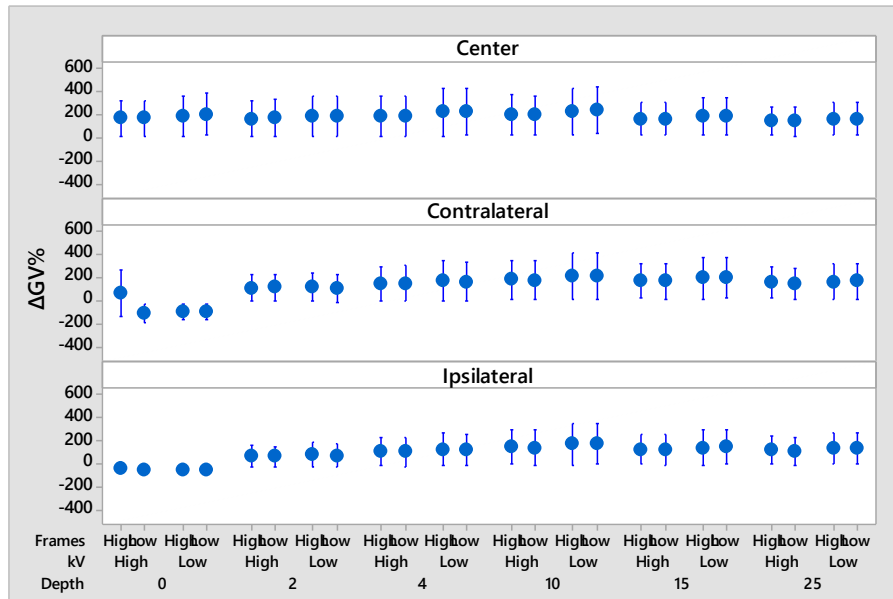


Figure 5 shows the overall plot of $\Delta\text{GV}\%$ (y-axis) for the 3D Accuitomo 170. As a trend, overall image quality ($\Delta\text{GV}\%$):

- Is reduced due to scatter (+ $\Delta\text{GV}\%$) for anterior cylinders similarly at all heights relative to the occlusal plane:
- Is reduced due to beam hardening (- $\Delta\text{GV}\%$) at the level of the occlusal plane for both ipsilateral and contralateral cylinders,
- Is reduced due to scatter is (+ $\Delta\text{GV}\%$) at levels below the occlusal plane for both ipsilateral and contralateral cylinders reaching a plateau at about 4mm,
- Appears to be independent of kV or number of projection frames.

Figure 6. 3D Accuitemo 170 interval plot showing $\Delta GV\%$ for each test cylinder location according to each independent variable (Depth, kV and resolution) according to position of the HDO relative to the test cylinder (adjacent vs. non-adjacent).

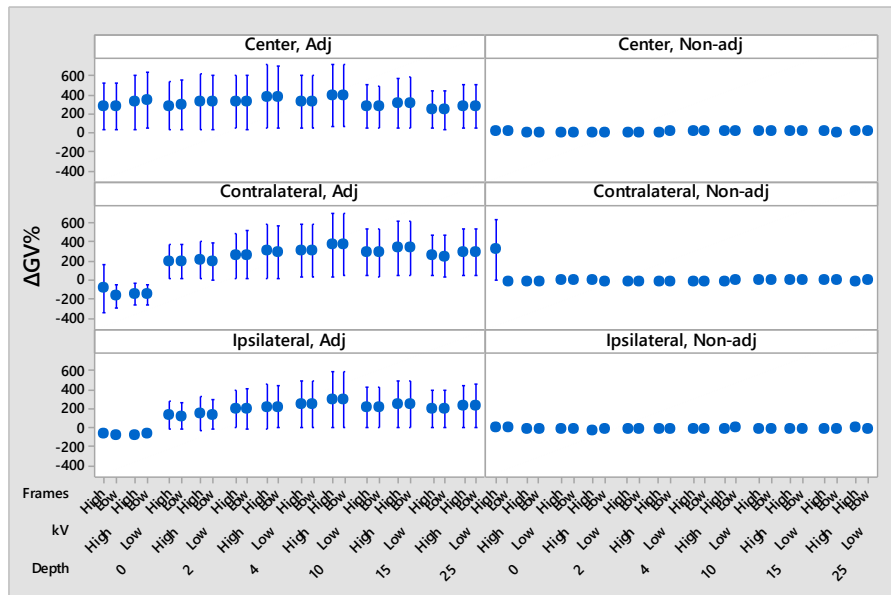


Figure 6 shows a plot of $\Delta GV\%$ (y-axis) according to position of the HDO relative to the test cylinder (adjacent vs. non-adjacent) for the 3D Accuitemo 170. As a trend, image quality ($\Delta GV\%$):

- Is highly dependent on the position of the HDO in that non-adjacent HDOs minimally affect image quality for anterior, ipsi- and contra-lateral sides.

2) Analytical

Multiple Analysis of Variance for Each CBCT Unit

Tables 9-31 shows the General Linear Model for each CBCT unit for the dependent variable, Δ GV%, grouped according to each independent variable.

CS 90003D

Table 9 shows that there is no overall effect from the arch type (maxilla mean Δ GV% = 12.7, mandible mean Δ GV% = 11.8; $T=-0.7072$, $p=0.48$) or sidedness (unilateral, bilateral). Therefore data from the maxillary and mandibular models can be combined and the effect of sidedness and arch ignored. Of the total variability, 76% is unexplained (Error SS). However, of the significant factors the most important, in order, are configuration (10.4%), arch location (6.6%), level of cylinder (4.7%), proximity (4.1%), resolution (1.6%) and, kV (0.7%).

Table 9. CS 90003D GLM

<i>Source</i>	<i>DF</i>	<i>SS</i>	<i>MS</i>	<i>F</i>	<i>Sig.</i>
Configuration	14	253284	18092	20.96	0.000
Level of Cylinder	5	112844	22569	26.15	0.000
Arch	1	432	432	0.50	0.480
Arch location	2	159866	79933	92.60	0.000
kV	1	16853	16853	19.53	0.000
Resolution	1	38211	38211	44.27	0.000
Sidedness	1	737	737	0.69	0.408
Proximity	1	99030	99030	92.12	0.000
Error	2135	1842868	863		
Total	2159	2424358			

GLM, General Linear Model; DF, degrees of freedom; SS, sum of the squares; MS, mean square; F, F value; Sig., statistical significance.

Post Hoc Analysis

Table 10 shows *Post Hoc* pairwise comparison for $\Delta GV\%$ at various configurations of HDO artifacts. The analysis indicates that overall there are no differences between specific artifact configurations within overlapping groups of increasing $\Delta GV\%$:

- Group (Configuration 12, 1, 15, 19 and 16) [Range; $\Delta GV\%$, 29.61 to 18.8],
- Group (Configuration 1, 15, 19, 16, 24, 18, 21, 5, 2 and 3) [Range; $\Delta GV\%$, 19.94 to 11.48],
- Group (Configuration 19, 16, 24, 18, 21, 5, 2 and 3) [Range; $\Delta GV\%$, 18.98 to 7.96],
- Group (Configuration 24, 18, 21, 5, 2, 3 and 9) [Range; $\Delta GV\%$, 17.32 to 6.59],
- Group (Configuration 5, 2, 3, 9 and 25) [Range; $\Delta GV\%$, 14.51 to 3.12],
- Group (Configuration 2, 3, 9, 25 and 6) [Range; $\Delta GV\%$, 11.48 to 0.27].
- Configuration 13 ($\Delta GV\%$, 17.83) is different from all other configurations.

Identifying trends within this series taking into account the proximity of the test cylinder to the HDO, whether the HDO was uni- or bilateral and number of HDOs indicates that configurations with the worst $\Delta GV\%$ are those test cylinders adjacent to the HDO or configurations that have the highest number of HDOs overall.

Table 10. *Post Hoc* pairwise comparison (Tukey) for Δ GV% for various configurations of HDO Artifact

<i>Pairwise Comparison</i>		<i>Analysis</i>			
Baseline	M.ean	Level	Mean	T-value	p
Config. 1	-19.94	Config. 5	-14.51	1.567	0.9656
		Config. 9	-6.59	3.855	0.0099
		Config. 2	-11.48	2.443	0.4820
		Config. 6	-0.27	5.681	0.0000
		Config. 3	-7.96	3.46	0.0401
		Config. 12	-29.61	-2.794	0.2498
		Config. 15	-19.91	0.009	1.0000
		Config. 16	-18.8	0.33	1.0000
		Config. 18	-17.28	0.766	1.0000
		Config. 19	-18.98	0.276	1.0000
		Config. 21	-15.82	1.189	0.9976
		Config. 13	17.83	-10.907	0.0000
		Config. 24	-17.32	0.756	1.0000
		Config. 25	-3.12	4.858	0.0002
Config. 5	-14.51	Config. 9	-6.59	2.288	0.5999
		Config. 2	-11.48	-0.876	0.9999
		Config. 6	-0.27	4.114	0.0036
		Config. 3	-7.96	-1.892	0.8574
		Config. 12	-29.61	4.361	0.0013
		Config. 15	-19.91	1.5584	0.9672
		Config. 16	-18.8	1.23793	0.9963
		Config. 18	-17.28	0.8010	1.0000
		Config. 19	-18.98	1.2914	0.9943
		Config. 21	-15.82	0.3787	1.0000
		Config. 13	17.83	-9.34	0.0000
		Config. 24	-17.32	0.8119	1.0000
		Config. 25	-3.12	-3.291	0.0683
		Config. 9	6.59	Config. 2	-11.48
Config. 6	-0.27			-1.826	0.8878
Config. 3	-7.96			0.395	1.0000
Config. 12	-29.61			6.649	0.0000
Config. 15	-19.91			3.8460	0.0103
Config. 16	-18.8			3.52550	0.0323
Config. 18	-17.28			3.0886	0.1215
Config. 19	-18.98			3.5790	0.0270
Config. 21	-15.82			2.6662	0.3258
Config. 13	17.83			-7.05	0.0000
Config. 24	-17.32			3.0995	0.1179
Config. 25	-3.12			-1.003	0.9996

Table 10 (continued). *Post Hoc* pairwise comparison (Tukey) for Δ GV% for various configurations of artifact

<i>Pairwise Comparison</i>		<i>Analysis</i>			
Baseline	Mean	Level	Mean	T-value	P
Config. 2	11.48	Config. 6	-0.27	3.238	0.0798
		Config. 3	-7.96	1.016	0.9996
		Config. 12	-29.61	5.237	0.0000
		Config. 15	-19.91	2.4345	0.4888
		Config. 16	-18.8	2.11396	0.7258
		Config. 18	-17.28	1.6771	0.9403
		Config. 19	-18.98	2.1675	0.6885
		Config. 21	-15.82	-1.255	0.9958
		Config. 13	17.83	-8.46	0.0000
		Config. 24	-17.32	-1.688	0.9372
Config. 6	0.27	Config. 25	-3.12	2.415	0.5037
		Config. 3	-7.96	2.221	0.6493
		Config. 12	-29.61	8.475	0.0000
		Config. 15	-19.91	5.6724	0.0000
		Config. 16	-18.8	5.35187	0.0000
		Config. 18	-17.28	4.9150	0.0001
		Config. 19	-18.98	5.4054	0.0000
		Config. 21	-15.82	4.4926	0.0007
		Config. 13	17.83	-5.23	0.0001
		Config. 24	-17.32	4.9259	0.0001
Config. 3	7.96	Config. 25	-3.12	-0.823	1.0000
		Config. 12	-29.61	6.254	0.0000
		Config. 15	-19.91	3.4509	0.0413
		Config. 16	-18.8	3.13042	0.1084
		Config. 18	-17.28	2.6935	0.3086
		Config. 19	-18.98	3.1839	0.0933
		Config. 21	-15.82	2.2711	0.6123
		Config. 13	17.83	-7.45	0.0000
		Config. 24	-17.32	2.7044	0.3019
		Config. 25	-3.12	-1.398	0.9877
Config. 12	29.61	Config. 15	-19.91	2.803	0.2449
		Config. 16	-18.8	3.124	0.1105
		Config. 18	-17.28	3.560	0.0287
		Config. 19	-18.98	3.070	0.1277
		Config. 21	-15.82	3.983	0.0061
		Config. 13	17.83	-13.701	0.0000
		Config. 24	-17.32	3.549	0.0298
		Config. 25	-3.12	7.652	0.0000

Table 10 (continued). *Post Hoc* pairwise comparison (Tukey) for Δ GV% for various configurations of artifact

<i>Pairwise Comparison</i>			<i>Analysis</i>		
Baseline	Mean	Level	Mean	T-value	p
Config. 15	19.91	Config. 16	-18.8	0.3205	1.0000
		Config. 18	-17.28	0.7574	1.0000
		Config. 19	-18.98	0.2670	1.0000
		Config. 21	-15.82	1.1798	0.9978
		Config. 13	17.83	-10.90	0.0000
		Config. 24	-17.32	0.7465	1.0000
Config. 16	-18.8	Config. 25	-3.12	4.8491	0.0002
		Config. 18	-17.28	0.43688	1.0000
		Config. 19	-18.98	-0.05350	1.0000
		Config. 21	-15.82	0.85927	0.9999
		Config. 13	17.83	-10.58	0.0000
Config. 18	-17.28	Config. 24	-17.32	0.42600	1.0000
		Config. 25	-3.12	4.52858	0.0006
		Config. 19	-18.98	-0.4904	1.0000
		Config. 21	-15.82	0.4224	1.0000
Config. 19	-18.98	Config. 13	17.83	-10.14	0.0000
		Config. 24	-17.32	-0.0109	1.0000
		Config. 25	-3.12	4.0917	0.0039
		Config. 21	-15.82	0.9128	0.9999
Config. 21	-15.82	Config. 13	17.83	-10.63	0.0000
		Config. 24	-17.32	0.4795	1.0000
		Config. 25	-3.12	4.5821	0.0005
Config. 13	-17.83	Config. 13	17.83	9.72	0.0000
		Config. 24	-17.32	-0.4333	1.0000
Config. 24	-17.32	Config. 25	-3.12	3.6693	0.0197
		Config. 24	-17.32	-10.15	0.0000
		Config. 25	-3.12	-6.05	0.0000
		Config. 25	-3.12	4.1026	0.0037

Config., configuration

Table 11 shows the *Post Hoc* pairwise comparison (Tukey) for Δ GV% at various levels of the cylinder. At the occlusal level (0mm), image quality (Δ GV%) is significantly worse than 4mm or greater at this level. At 2mm from the occlusal level (2mm), HDOs significantly affect Δ GV% values 10 mm and above. At 4mm from the occlusal level (4mm), image quality (Δ GV%) is significantly worse than 15 mm and above. At the 10mm level from the occlusal level (10mm), there is no difference between artifacts at the 4mm level or higher at the 15 and 25mm levels.

Table 11. *Post Hoc* pairwise comparison (Tukey) for Δ GV% at various level of cylinder

<i>Pairwise Comparison</i>			<i>Analysis</i>		
Baseline	Mean	Level	Mean	T-value	p
Occlusal (0mm)	-23.85	2	-18.99	2.218	0.229
		4	-13.3	4.817	0.000
		10	-7.13	7.635	0.000
		15	-6.66	7.846	0.000
		25	-3.59	9.251	0.000
2mm	-18.99	4	-13.3	2.59	0.0975
		10	-7.13	5.417	0.000
		15	-6.66	5.627	0.000
		25	-3.59	7.033	0.000
4mm	-13.3	10	-7.13	2.818	0.0546
		15	-6.66	3.029	0.0296
		25	-3.59	4.434	0.000
10mm	-7.13	15	-6.66	0.21	0.999
		25	-3.59	1.616	0.5878
15mm	-6.66	25	-3.59	1.406	0.7237

Table 12 shows the *Post Hoc* pairwise comparison for Δ GV% at various arch locations. The Δ GV% at different arch locations are all significantly different from each other with minimal overall loss in image quality in the center, more on the contralateral side and the greatest in the ipsilateral side.

Table 12. *Post Hoc* pairwise comparison (Tukey) for Δ GV% at various arch locations

<i>Pairwise Comparison</i>			<i>Analysis</i>		
Baseline	Mean	Level	Mean	T-value	P
Center	-1.18	Ipsilateral	-22.16	-13.55	0.000
		Contralateral	-13.4	-7.9	0.000
Ipsilateral	-22.16	Contralateral	-13.4	-5.65	0.000

Table 13 shows *Post Hoc* pairwise comparison for Δ GV% at two kVs. Overall, images performed at 90kV produce a significantly worse image quality than at 75kV.

Table 13. *Post Hoc* pairwise comparison (Tukey) for Δ GV% at two kV levels.

<i>Pairwise Comparison</i>			<i>Analysis</i>		
Baseline	Mean	Level	Mean	T-value	p
75 kV	-9.46	90 kV	-15.04	4.419	0.000

Table 14 shows the *Post Hoc* pairwise comparison for Δ GV% at various resolutions. Overall images obtained at higher resolution (0.076mm) provide a greater loss in image quality than at low resolution (0.2mm).

Table 14. *Post Hoc* pairwise comparison (Tukey) for Δ GV% at high and low resolutions.

<i>Pairwise Comparison</i>			<i>Analysis</i>		
Baseline	Mean	Level	Mean	T-Value	P
Hi Res	-16.46	Low Res	-8.05	6.65	0.000

Table 15 shows the *Post Hoc* pairwise comparison for Δ GV% according to

whether HDO are uni- or bilaterally positioned and shows that image quality is independent of position of HDO.

Table 15. *Post Hoc* pairwise comparison (Tukey) for Δ GV% according to the side where HDO is positioned.

<i>Pairwise Comparison</i>			<i>Analysis</i>		
Baseline	Mean	Level	Mean	T-Value	P
Unilateral	-10.12	Bilateral	-11.33	0.8277	0.4078

Table 16 shows *Post Hoc* pairwise comparison for Δ GV% at position of HDO relative to test cylinder. Overall images with HDOs positioned adjacent to test cylinder show significantly greater loss in image quality than images with HDOs non-adjacent to test cylinder.

Table16. *Post Hoc* pairwise comparison (Tukey) for Δ GV% at position of HDMO relative to test cylinder

<i>Pairwise Comparison</i>			<i>Analysis</i>		
Baseline	Mean	Level	Mean	T-Value	P
Non-adjacent	-3.72	Adjacent	-17.74	9.598	0.000

iCAT Next Generation

Table 17 shows that all factors significantly affect image quality (Δ GV%). Of the total variability, 20.9% is unexplained (Error SS). The most important factors, in order, are configuration (74.6%), proximity (12.9%), sidedness (12.1%), level of cylinder (3%), arch location (1.1%), resolution (0.2%), and finally arch (0.18%).

Table 17. Analysis of Variance for iCAT Next Generation

<i>Source</i>	<i>DF</i>	<i>SS</i>	<i>MS</i>	<i>F</i>	<i>Sig.</i>
Configuration	14	127092974	9078070	268.87	0.000
Level of Cylinder	5	5181565	1036313	30.69	0.000
Arch	1	314102	314102	9.30	0.002
Arch location	2	1829191	914596	27.09	0.000
Resolution	1	378076	378076	11.20	0.001
Sidedness	1	20590531	20590531	185.89	0.000
Proximity	1	22039565	22039565	198.97	0.000
Error	1056	35654947	33764		
Total	1079	170450855			

GLM, General Linear Model; DF, degrees of freedom; SS, sum of the squares; MS, mean square; F, F value; Sig., statistical significance.

Post Hoc Analysis

Table 18 shows *Post Hoc* pairwise comparison for Δ GV% at various configurations of HDOs. Overall there are differences between specific artifacts configurations within 3 groups of increasing Δ GV%:

- Group (Configuration 24, 21, 6, 12, 3, 1, 5, 13, 2, 25 and 9) [Range Δ GV%, -49.31 to -1.14],
- Group (Configuration 18) [Δ GV%, 639.96],
- Group (Configuration 19, 15 and 16) [Range Δ GV%, 775.59 to 810.90].

Identifying trends within this series, taking into consideration proximity of the test cylinder to the HDMO, whether the HDMO was uni- or bilateral and number of HDMOs indicates that configurations with the worst Δ GV% are those test cylinders adjacent to the HDO or that have the highest number of HDOs overall.

Table 18. *Post Hoc* pairwise comparison (Tukey) for Δ GV% for various configurations of HDOs

<i>Pairwise Comparison</i>			<i>Analysis</i>				
Baseline	Mean	Level	Mean	T-value	P		
Config. 1	16.68	Config. 5	-15.94	0.024	1.0000		
		Config. 9	-1.14	0.507	1.0000		
		Config. 2	-6.26	0.340	1.0000		
		Config. 6	-21.75	-0.166	1.0000		
		Config. 3	-19.18	-0.082	1.0000		
		Config. 12	-21.21	-0.148	1.0000		
		Config. 15	786.66	26.231	0.0000		
		Config. 16	810.90	27.023	0.0000		
		Config. 18	639.96	21.441	0.0000		
		Config. 19	775.59	25.870	0.0000		
		Config. 21	-33.67	-0.555	1.0000		
		Config. 13	-9.99	0.218	1.0000		
		Config. 24	-49.31	-1.066	0.9993		
		Config. 25	-4.11	0.410	1.0000		
		Config. 5	-15.94	Config. 9	-1.14	0.4833	1.0000
Config. 2	-6.26			-0.316	1.0000		
Config. 6	-21.75			-0.1897	1.0000		
Config. 3	-19.18			0.10569	1.0000		
Config. 12	-21.21			0.1722	1.0000		
Config. 15	786.66			-26.21	0.0000		
Config. 16	810.90			-27.00	0.0000		
Config. 18	639.96			-21.42	0.0000		
Config. 19	775.59			-25.85	0.0000		
Config. 21	-33.67			0.5790	1.0000		
Config. 13	-9.99			-0.194	1.0000		
Config. 24	-49.31			1.0897	0.9991		
Config. 25	-4.11			-0.3862	1.0000		
Config. 9	-1.14			Config. 2	-6.26	0.167	1.0000
				Config. 6	-21.75	0.6730	1.0000
		Config. 3	-19.18	0.58901	1.0000		
		Config. 12	-21.21	0.6555	1.0000		
		Config. 15	786.66	-25.72	0.0000		
		Config. 16	810.90	-26.52	0.0000		
		Config. 18	639.96	-20.93	0.0000		
		Config. 19	775.59	-25.36	0.0000		
		Config. 21	-33.67	1.0623	0.9993		
		Config. 13	-9.99	0.289	1.0000		
		Config. 24	-49.31	1.5731	0.9645		

Table 18(Continued). *Post Hoc* pairwise comparison (Tukey) for Δ GV% for various configurations of HDOs

<i>Pairwise Comparison</i>		<i>Analysis</i>			
Baseline	Mean	Level	Mean	T-value	P
Config. 2	-6.26	Config. 25	-4.11	0.0971	1.0000
		Config. 6	-21.75	-0.506	1.0000
		Config. 3	-19.18	-0.422	1.0000
		Config. 12	-21.21	0.4884	1.0000
		Config. 15	786.66	-25.89	0.0000
		Config. 16	810.90	-26.68	0.0000
		Config. 18	639.96	-21.10	0.0000
		Config. 19	775.59	-25.53	0.0000
		Config. 21	-33.67	-0.895	0.9999
		Config. 13	-9.99	0.122	1.0000
		Config. 24	-49.31	-1.406	0.9870
Config. 6	-21.75	Config. 25	-4.11	0.070	1.0000
		Config. 3	-19.18	-0.08397	1.0000
		Config. 12	-21.21	-0.0175	1.0000
		Config. 15	786.66	-0.384	0.0000
		Config. 16	810.90	-27.19	0.0000
		Config. 18	639.96	-21.61	0.0000
		Config. 19	775.59	-26.04	0.0000
		Config. 21	-33.67	-0.5108	1.0000
		Config. 13	-9.99	-0.384	1.0000
		Config. 24	-49.31	0.9001	0.9999
		Config. 25	-4.11	-0.5759	1.0000
Config. 12	-21.21	Config. 16	810.90	-27.10	0.0000
		Config. 18	639.96	-21.52	0.0000
		Config. 19	775.59	-25.95	0.0000
		Config. 21	-33.67	0.4733	1.0000
		Config. 13	-9.99	-0.300	1.0000
		Config. 24	-49.31	0.9841	0.9997
		Config. 25	-4.11	-0.4919	1.000
		Config. 15	786.66	26.3795	0.0000
		Config. 16	810.90	27.1712	0.0000
		Config. 18	639.96	21.5893	0.0000
		Config. 19	775.59	26.0182	0.0000
Config. 21	-33.67	-0.4068	1.0000		
Config. 13	-9.99	0.3664	1.0000		
Config. 24	-49.31	-0.9176	0.9999		

Table 18(Continued). *Post Hoc* pairwise comparison (Tukey) for Δ GV% for various configurations of HDOs

<i>Pairwise Comparison</i>		<i>Analysis</i>			
Baseline	Mean	Level	Mean	T-value	P
Config. 15	786.66	Config. 25	-4.11	0.5584	1.0000
		Config. 16	810.90	0.79	1.0000
		Config. 18	639.96	-4.79	0.0002
		Config. 19	775.59	-0.36	1.0000
		Config. 21	-33.67	-26.79	0.0000
		Config. 13	-9.99	26.013	0.0000
		Config. 24	-49.31	-27.30	0.0000
Config. 16	810.90	Config. 25	-4.11	-25.82	0.0000
		Config. 18	639.96	-5.58	0.0000
		Config. 19	775.59	-1.15	0.9983
		Config. 21	-33.67	-27.58	0.0000
		Config. 13	-9.99	26.805	0.0000
		Config. 24	-49.31	-28.09	0.0000
Config. 18	639.96	Config. 25	-4.11	-26.61	0.0000
		Config. 19	775.59	4.43	0.0009
		Config. 21	-33.67	-22.00	0.0000
		Config. 13	-9.99	21.223	0.0000
		Config. 24	-49.31	-22.51	0.0000
Config. 19	775.59	Config. 25	-4.11	-21.03	0.0000
		Config. 21	-33.67	-26.42	0.0000
		Config. 13	-9.99	25.652	0.0000
		Config. 24	-49.31	-26.94	0.0000
Config. 21	-33.67	Config. 25	-4.11	-25.46	0.0000
		Config. 13	-9.99	-0.773	1.0000
		Config. 24	-49.31	-0.5108	1.0000
Config. 13	-9.99	Config. 25	-4.11	0.9652	0.9998
		Config. 24	-49.31	-1.284	0.9946
Config. 24	-49.31	Config. 25	-4.11	0.192	1.0000
Config. 24	-49.31	Config. 25	-4.11	1.4760	0.9797

Config., configuration

Table 19 shows the *Post Hoc* pairwise comparison (Tukey) for Δ GV% at various levels of cylinder relative to the occlusal plane. At the occlusal level (0mm), image quality significantly differs from Δ GV% values at all other levels. At 2mm from the occlusal level (2mm), image quality significantly differs from Δ GV% values at 10 and 15mm. At levels 4mm apical from the occlusal plane (4mm, 10mm, 15mm, 25mm), image quality does not significantly differ from Δ GV% values at any level apical to 10mm.

Table 19. *Post Hoc* pairwise comparison (Tukey) for Δ GV% at various level of cylinder

<i>Pairwise Comparison</i>	<i>Mean</i>	<i>Level</i>	<i>Mean</i>	<i>Analysis</i>	
				<i>T-value</i>	<i>P</i>
<i>Baseline</i>					
Occlusal (0mm)	42.07	2	173.09	6.764	0.0000
		4	217.40	9.052	0.0000
		10	250.45	10.758	0.0000
		15	233.36	9.876	0.0000
		25	209.17	8.627	0.0000
2mm	173.09	4	217.40	2.288	0.1990
		10	250.45	-3.994	0.0009
		15	233.36	-3.111	0.0229
		25	209.17	-1.863	0.4253
4mm	217.40	10	250.45	-1.706	0.5274
		15	233.36	-0.824	0.9632
		25	209.17	0.425	0.9982
10mm	250.45	15	233.36	-0.883	0.9508
		25	209.17	-2.131	0.2710
15mm	233.36	25	209.17	-1.249	0.8127

Table 20 shows the *Post Hoc* pairwise comparison for Δ GV% at various arch locations. The Δ GV% values in the anterior portion of the arch (Center) are significantly higher from ipsilateral and contralateral locations which are similar.

Table 20. *Post Hoc* pairwise comparison (Tukey) for Δ GV% at various arch locations

<i>Pairwise Comparison</i>			<i>Analysis</i>		
Baseline	Mean	Level	Mean	T-value	p
Center	245.78	Ipsilateral	157.38	-6.455	0.0000
		Contralateral	159.62	-6.291	0.0000
Ipsilateral	157.38	Contralateral	159.62	-0.1636	0.9854

Table 21 shows the *Post Hoc* pairwise comparison for Δ GV% at various resolutions. Overall images performed at a high resolution (0.076mm) provide significantly less artifacts than at a low resolution (0.2mm).

Table 21. *Post Hoc* pairwise comparison (Tukey) for Δ GV% at two resolutions.

<i>Pairwise Comparison</i>			<i>Analysis</i>		
Baseline	Mean	Level	Mean	T-value	p
Low	206.30	High	168.88	3.346	0.0008

Table 22 shows the *Post Hoc* pairwise comparison for Δ GV% for different arches. Overall images performed for the maxillary arch have better image quality than for the mandibular arch.

Table 22. *Post Hoc* pairwise comparison (Tukey) for Δ GV% at two arches

<i>Pairwise Comparison</i>			<i>Analysis</i>		
Baseline	Mean	Level	Mean	T-value	p
Maxillary	170.54	Mandibular	204.65	-3.050	0.0023

Table 23 shows the *Post Hoc* pairwise comparison for Δ GV% according to side of

HDO in the respective arch. Overall images performed with HDOs bilaterally result in significantly greater reduction in image quality due to scatter (+ Δ GV%) than with unilaterally positioned HDOs.

Table 23. *Post Hoc* pairwise comparison (Tukey) for Δ GV% according to side of HDO

<i>Pairwise Comparison</i>			<i>Analysis</i>		
Baseline	Mean	Level	Mean	T-value	p
Unilateral	-13.49	Bilateral	272.36	-13.63	0.0000

Table 24 shows the *Post Hoc* pairwise comparison for Δ GV% according to proximity of HDMO to the test cylinder in the arch. Overall images with HDOs adjacent to test cylinder provide significantly worse image quality due to scatter (+ Δ GV%) than images with HDOs positioned non-adjacent to test cylinder.

Table 24. *Post Hoc* pairwise comparison (Tukey) for Δ GV% according to proximity of HDMO to test cylinder.

<i>Pairwise Comparison</i>			<i>Analysis</i>		
Baseline	Mean	Level	Mean	T-value	p
Non-adjacent	-18.43	Adjacent	277.30	-14.11	0.0000

3D Accuitomo 170

Based on the MANOVA from Table X there is no overall effect from kV (90 kV mean Δ GV%, 128.71; 75 kV mean Δ GV%, 144.77) or number of frames (High # of frames mean Δ GV%, 139.46; Low # of frames mean Δ GV%, 134.02). Therefore data from the these independent variables can be combined and *Post Hoc* analysis is unnecessary.

Of the total variability, 28.2% is unexplained (Error SS). The most important factors, in order, are configuration (69%), proximity (5.9%), sidedness (5.3%), level of cylinder (1.8%), arch location (0.7%) and, finally, arch (0.2%).

Table 25. 3D Accuitomo 170 Analysis of Variance

<i>Source</i>	<i>DF</i>	<i>SS</i>	<i>MS</i>	<i>F</i>	<i>Sig.</i>
Configuration	14	236794854	16913918	372.71	0.000
Level of Cylinder	5	6085359	1217072	26.82	0.000
Arch	1	592607	592607	13.06	0.000
Arch location	2	2564759	1282379	28.26	0.000
kV	1	139400	139400	3.07	0.080
Frames	1	15949	15949	0.35	0.553
Sidedness	1	18154387	18154387	131.79	0.000
Proximity	1	20152425	20152425	146.30	0.000
Error	2135	96889199	45381		
Total	2159	343082127			

DF, degrees of freedom; SS, sum of the squares; MS, mean square; F, F value; Sig., statistical significance

Post Hoc Analysis

Table 26 shows *Post Hoc* pairwise comparison for $\Delta\text{GV}\%$ at various HDO configurations. The analysis shows that overall there are no differences between specific artifacts configurations within 4 groups of increasing $\Delta\text{GV}\%$:

- Group (Configuration 24, 21, 12, 1, 13, 9, 25, 6, 5, 3 and 2) [Range $\Delta\text{GV}\%$, -33.00 to 9.17],
- Group (Configuration 13, 9, 25, 6, 5, 3, 2, 19 and 18) [Range $\Delta\text{GV}\%$, -2.59 to 81.25],
- Configuration 15 ($\Delta\text{GV}\%$, 908.13) and configuration 16 ($\Delta\text{GV}\%$, 1041.63) are each different from all other configurations.

Identifying trends within this series, taking into consideration the proximity of the test cylinder to the HDO, whether the HDO was uni- or bilateral and number of HDOs indicates that configurations with the worst $\Delta\text{GV}\%$ are those test cylinders adjacent to the HDO or who have the highest number of HDOs overall.

Table 26. *Post Hoc* pairwise comparison (Tukey) for Δ GV% for various configurations of Artifacts

<i>Pairwise Comparison</i>			<i>Analysis</i>		
Baseline	Mean	Level	Mean	T-value	p
Config. 1	-9.92	Config. 5	5.97	0.6330	1.0000
		Config. 9	-1.88	0.3201	1.0000
		Config. 2	9.17	0.7603	1.0000
		Config. 6	5.33	0.6073	1.0000
		Config. 3	8.55	0.7358	1.0000
		Config. 12	-16.97	-0.2808	1.0000
		Config. 15	908.13	36.5673	0.0000
		Config. 16	1041.63	41.8849	0.0000
		Config. 18	81.25	3.6313	0.0225
		Config. 19	79.56	3.5640	0.0284
		Config. 21	-23.36	-0.5354	1.0000
		Config. 13	-2.59	0.2920	1.0000
		Config. 24	-33.00	-0.9194	0.9999
		Config. 25	-0.75	0.3651	1.0000
Config. 5	14.51	Config. 9	-1.88	-0.3129	1.000
		Config. 2	9.17	-0.127	1.0000
		Config. 6	5.33	-0.0257	1.000
		Config. 3	8.55	-0.1027	1.000
		Config. 12	-16.97	0.9139	0.9999
		Config. 15	908.13	-35.93	0.0000
		Config. 16	1041.63	-41.25	0.0000
		Config. 18	81.25	-2.998	0.1539
		Config. 19	79.56	-2.931	0.1820
		Config. 21	-23.36	1.1684	0.9980
		Config. 13	-2.59	0.341	1.0000
		Config. 24	-33.00	1.552	0.9683
		Config. 25	-0.75	0.26794	1.000
		Config. 9	6.59	Config. 2	9.17
Config. 6	5.33			-0.2872	1.000
Config. 3	8.55			-0.4157	1.0000
Config. 12	-16.97			0.6009	1.0000
Config. 15	908.13			-36.25	0.0000
Config. 16	1041.63			-41.56	0.0000
Config. 18	81.25			-3.311	0.0641
Config. 19	79.56			-3.244	0.0784
Config. 21	-23.36			0.8555	0.9999
Config. 13	-2.59			0.028	1.0000
Config. 24	-33.00			1.240	0.9963

Table 26(Continued). *Post Hoc* pairwise comparison (Tukey) for Δ GV% for various configurations of Artifacts

<i>Pairwise Comparison</i>			<i>Analysis</i>		
Baseline	Mean	Level	Mean	T-value	p
Config. 2	11.48	Config. 25	-0.75	-0.04498	1.000
		Config. 6	5.33	-0.153	1.0000
		Config. 3	8.55	-0.025	1.0000
		Config. 12	-16.97	1.0411	0.9994
		Config. 15	908.13	-35.81	0.0000
		Config. 16	1041.63	-41.12	0.0000
		Config. 18	81.25	-2.871	0.2099
		Config. 19	79.56	-2.804	0.2445
		Config. 21	-23.36	-1.296	0.9941
		Config. 13	-2.59	0.468	1.0000
Config. 6	0.27	Config. 24	-33.00	-1.680	0.9395
		Config. 25	-0.75	-0.395	1.0000
		Config. 3	8.55	-0.1285	1.000
		Config. 12	-16.97	0.8882	0.9999
		Config. 15	908.13	-35.96	0.0000
		Config. 16	1041.63	-41.28	0.0000
		Config. 18	81.25	-3.024	0.1441
		Config. 19	79.56	-2.957	0.1708
		Config. 21	-23.36	1.1427	0.9984
		Config. 13	-2.59	0.315	1.0000
Config. 3	7.96	Config. 24	-33.00	1.527	0.9725
		Config. 25	-0.75	0.24223	1.000
		Config. 12	-16.97	1.0166	0.9996
		Config. 15	908.13	-35.83	0.0000
		Config. 16	1041.63	-41.15	0.0000
		Config. 18	81.25	-2.896	0.1982
		Config. 19	79.56	-2.828	0.2315
		Config. 21	-23.36	1.2712	0.9952
		Config. 13	-2.59	0.444	1.0000
		Config. 24	-33.00	1.655	0.9461
Config. 12	29.61	Config. 25	-0.75	0.37068	1.0000
		Config. 15	908.13	36.8482	0.0000
		Config. 16	1041.63	42.1658	0.0000
		Config. 18	81.25	3.9121	0.0080
		Config. 19	79.56	3.8449	0.0103
		Config. 21	-23.36	-0.2546	1.0000
		Config. 13	-2.59	0.5729	1.0000

Table 26(Continued). *Post Hoc* pairwise comparison (Tukey) for Δ GV% for various configurations of Artifacts

<i>Pairwise Comparison</i>		<i>Analysis</i>			
Baseline	Mean	Level	Mean	T-value	p
Config. 15	19.91	Config. 24	-33.00	-0.6386	1.0000
		Config. 25	-0.75	0.6459	1.0000
		Config. 16	1041.63	5.32	0.0000
		Config. 18	81.25	-32.94	0.0000
		Config. 19	79.56	-33.00	0.0000
		Config. 21	-23.36	-37.10	0.0000
		Config. 13	-2.59	36.275	0.0000
Config. 16	18.8	Config. 24	-33.00	-37.49	0.0000
		Config. 25	-0.75	-36.20	0.0000
		Config. 18	81.25	-38.25	0.0000
		Config. 19	79.56	-38.32	0.0000
		Config. 21	-23.36	-42.42	0.0000
		Config. 13	-2.59	41.593	0.0000
		Config. 24	-33.00	-42.80	0.0000
Config. 18	17.28	Config. 25	-0.75	-41.52	0.0000
		Config. 19	79.56	-0.067	1.0000
		Config. 21	-23.36	-4.167	0.0029
		Config. 13	-2.59	3.339	0.0589
		Config. 24	-33.00	-4.551	0.0006
		Config. 25	-0.75	-3.266	0.0734
		Config. 21	-23.36	-4.099	0.0038
Config. 19	18.98	Config. 13	-2.59	3.272	0.0722
		Config. 24	-33.00	-4.483	0.0007
		Config. 25	-0.75	-3.199	0.0894
		Config. 13	-2.59	-0.827	1.0000
		Config. 24	-33.00	-0.3841	1.0000
		Config. 25	-0.75	0.9005	0.9999
		Config. 24	-33.00	-1.211	0.9970
Config. 13	17.83	Config. 25	-0.75	0.073	1.0000
		Config. 24	-33.00	-1.211	0.9970
Config. 24	17.32	Config. 25	-0.75	1.285	0.9946

Config., configuration

Table 27 shows the *Post Hoc* pairwise comparison (Tukey) for Δ GV% at various levels of cylinder. At the occlusal level (0mm), Δ GV% values are significantly lower than at all other levels. At 2mm from the occlusal level (2mm), Δ GV% values are significantly lower than Δ GV% values at 10 mm. At levels 4mm and above from the occlusal plane (4mm, 10mm, 15mm, 25mm), Δ GV% values are not significantly different from Δ GV% values at any other more distant level.

Table 27. *Post Hoc* pairwise comparison (Tukey) for Δ GV% at various levels of cylinder

<i>Pairwise Comparison</i>			<i>Analysis</i>		
Baseline	Mean	Level	Mean	T-value	p
Occlusal (0mm)	27.65	2	123.58	6.042	0.000
		4	162.24	8.477	0.000
		10	192.97	10.412	0.000
		15	166.92	8.771	0.000
		25	147.09	7.522	0.000
2mm	123.58	4	162.24	2.435	0.1442
		10	192.97	4.370	0.0002
		15	166.92	2.729	0.0696
		25	147.09	1.481	0.6766
4mm	162.24	10	192.97	1.9351	0.3805
		15	166.92	0.2944	0.9997
		25	147.09	-0.9542	0.9321
10mm	192.97	15	166.92	-1.641	0.5714
		25	147.09	-2.889	0.0447
15mm	166.92	25	147.09	-1.249	0.8127

Table 28 shows the *Post Hoc* pairwise comparison for Δ GV% at various arch locations. The Δ GV% at different arch locations are all significantly different from each other with ipsilateral values less than contralateral values which are less than center values overall.

Table 28. *Post Hoc* pairwise comparison (Tukey) for Δ GV% at various arch locations

<i>Pairwise Comparison</i>			<i>Analysis</i>		
Baseline	Mean	Level	Mean	T-value	p
Center	182.54	Ipsilateral	99.41	13.55	0.000
		Contralateral	128.27	7.9	0.000
Ipsilateral	99.41	Contralateral	128.27	5.65	0.0274

Table 29 shows the *Post Hoc* pairwise comparison between arches for Δ GV%. Overall image quality for the maxillary arch is significantly better than the mandibular arch.

Table 29. *Post Hoc* pairwise comparison (Tukey) for Δ GV% at two arches

<i>Pairwise Comparison</i>			<i>Analysis</i>		
Baseline	Mean	Level	Mean	T-value	p
Maxillary	120.18	Mandibular	153.30	-3.614	0.0003

Table 30 shows the *Post Hoc* pairwise comparison for Δ GV% according to side of HDO in the arch. Overall images with HDOs bilaterally have significantly poorer quality than those with HDOs unilaterally.

Table 30. *Post Hoc* pairwise comparison (Tukey) for Δ GV% according to side of HDO in the arch

<i>Pairwise Comparison</i>			<i>Analysis</i>		
Baseline	Mean	Level	Mean	T-value	p
Unilateral	2.870	Bilateral	192.661	-11.48	0.0000

Table 31 shows the *Post Hoc* pairwise comparison for Δ GV% according to proximity of HDO to the test cylinder in the arch. Overall image quality is significantly improved when HDOs are not positioned adjacent to the test cylinder.

Table 31. *Post Hoc* pairwise comparison (Tukey) for Δ GV% according to proximity of HDO to test cylinder.

<i>Pairwise Comparison</i>			<i>Analysis</i>		
Baseline	Mean	Level	Mean	T-value	p
Non-adjacent	-2.215	Adjacent	197.747	-12.10	0.0000

CHAPTER V

DISCUSSION

The purpose of this study was to characterize the effect of artifacts due to the presence of coronal high density objects (HDO) in the dental arches on image quality. Since dental amalgam is the most commonly found HDO in the mouth, this project used coronal MOD amalgam preparations to study the beam hardening and scatter effects on radiographic images taken with different exposure parameters.

The model was constructed to simulate the radiographic appearance of the oral cavity as closely as possible. Measured gray values, at specific locations, were compared with gray values of control models (without any HDO) to arrive at $\Delta GV\%$ which could be statistically compared with each other. $\Delta GV\%$ was thus used as an index of image quality. $\Delta GV\%$ value of 0 meant HDOs had no significant effect on the image quality. + $\Delta GV\%$ values meant that images were lighter than control images and were thus affected by scatter. - $\Delta GV\%$ values indicated that images were affected by beam hardening and were darker than control images. Using these values as a reference, conclusions were drawn on whether an independent variable affected the image quality.

Each CBCT system (CS 9000 3D, iCAT Next Generation and Accuitomo 170) has differences in data acquisition that make unit comparisons problematic. The CS 9000 has a small, fixed FOV with an incomplete trajectory arc, fixed number of frames but variable mA and kV; The iCAT Next Generation has a variable FOV, complete trajectory

arc, variable number of frames but fixed mA and fixed but high kV. Finally the 3D Accuitomo 170 has a variable FOV, complete trajectory arc, variable number of frames but variable mA and kV. Overall the CS 9000 3D showed characteristic differences from the iCAT NG and Accuitomo 170, which both demonstrated similar trends.

The CS 9000 3D was the only CBCT unit where most of the variability (78%) was due to unknown sources. In addition, it was the only unit where the arch (maxilla/mandible) or sidedness (unilateral/ bilateral) did not have a significant effect on image quality. The worst beam hardening affected areas were occlusal 4mm of the ipsilateral cylinder with maximum number of HDOs. Scatter did not play a major role in CS 9000 3D images, except for when HDOs were non-adjacent to the test cylinder and scanned at a high resolution. Contradictory to expectations, a higher kV resulted in poorer image quality than at a lower kV. Future research could possibly be done to explain this phenomenon.

Images scanned with iCAT NG exhibited greater deterioration of image quality by scatter rather than beam hardening. Occlusal (0mm) - 2mm of ipsilateral and contralateral test cylinders with adjacent HDOs were most affected by beam hardening while all other levels showed predominantly scatter artifacts. This is probably because all images were scanned at 120kV, which is higher than any other system. Beam hardening effects by HDOs at high kV is less than at lower kVs. Image quality adjacent to HDOs with bilaterally positioned HDOs scanned at lower resolution were deteriorated by scatter while non- adjacent, unilaterally positioned HDOs scanned at a higher resolution were affected by beam hardening artifacts. Both arches showed significant scatter effects.

For the 3D Accuitomo 170, kV and number of frames were not found to have a

significant effect on the quality of images overall. Similar to the iCAT NG, images scanned with this system were more affected by scatter artifacts. Beam hardening artifacts were seen at the occlusal (0mm) – 2mm of the ipsilateral and contralateral cylinders of adjacent HDOs. Image quality deteriorated by adjacent, bilaterally positioned HDOs due to scatter while image quality due to beam hardening was minimally affected by non- adjacent positioned HDOs. Both dental arches showed significant scatter effects overall.

There are some limitations in this study in that the *in-vitro* model design does not completely replicate the human dental arch form. In addition this study included only posterior HDOs (dental amalgam) and did not involve other coronal restorative materials such as composite resin, porcelain or complete crowns.

Previous studies that have stated that caries detection is better in CBCT images than intraoral radiographic images have not taken into account the presence of HDOs.^(5, 9, 14, 15) This study clearly demonstrates that HDO degrades image quality particularly if they are adjacent to an unrestored coronal area. Clinicians should be aware that this degradation due to the presence of HDO may invalidate the results of these authors. In particular, the results of this study indicate that there is extensive image degradation in the occlusal 4mm range of the coronal aspect of the dentition teeth due to beam hardening streak artifacts

There are numerous areas for future research. Additional studies should substitute teeth with various degrees of coronal dental caries for the control cylinders in the current model and investigate the effect of various HDO configurations in dental caries detection. Materials other than dental amalgam should also be used as HDOs. Much of the

significant variability of the CS 9000 3D is unexplained and not due to CBCT operational parameters or HDO configuration. This was unexpected and should be the subject of further research. In addition unexpected results were found for the 3D Accuitomo 170 in that there was no overall effect from increases in kV (from 75 kV to 90 kV) or number of frames, both of which should have improved image quality. Sub-analysis of the data for specific HDO configurations should be performed for this CBCT unit.

CHAPTER VI

CONCLUSION

Within the limitations of this *in-vitro* study, it can be concluded that:

- HDOs present in the dental arches cause beam hardening and scatter artifacts and reduce image quality due to increasing noise.
- These artifacts are present not only the ipsilateral side but also the contralateral side and anterior region. In other words, HDOs cause artifacts in all areas of the oral cavity, either through beam hardening or scatter artifacts.
- Beam hardening streak artifacts are predominantly seen in the occlusal 4mm range of the coronal aspect of the dentition. Scatter artifacts usually predominate more apical to the 4mm level.
- Because of the degradation effects of HDO on image quality in the coronal aspect of the dentition, the detection of dental caries on CBCT images in patients with restorations should be viewed with caution. The results of this study suggests that dental caries diagnosis in the presence of HDOs could be either be missed by scatter artifacts or misdiagnosed (false positive) due to beam hardening artifacts.

REFERENCES

1. Schulze RKW, Berndt D, D'Hoedt B. On cone-beam computed tomography artifacts induced by titanium implants. *Clinical Oral Implants Research*. 2010;21(1):100-7.
2. Benic GI, Sancho-Puchades M, Jung RE, Deyhle H, Hämmerle CHF. In vitro assessment of artifacts induced by titanium dental implants in cone beam computed tomography. *Clinical Oral Implants Research*. 2012:n/a-n/a.
3. Naitoh M, Saburi K, Gotoh K, Kurita K, Arijii E. Metal Artifacts From Posterior Mandibular Implants as Seen in CBCT. *Implant dentistry*. 2013 Apr;22(2):151-4.
4. Ritter L, Mischkowski RA, Neugebauer J, Dreiseidler T, Scheer M, Keeve E, et al. The influence of body mass index, age, implants, and dental restorations on image quality of cone beam computed tomography. *Oral Surgery, Oral Medicine, Oral Pathology, Oral Radiology, and Endodontology*. 2009 9//;108(3):e108-e16.
5. Akdeniz BG, Grondahl HG, Magnusson B. Accuracy of proximal caries depth measurements: comparison between limited cone beam computed tomography, storage phosphor and film radiography. *Caries research*. 2006;40(3):202-7.
6. Tsuchida R, Araki K, Okano T. Evaluation of a limited cone-beam volumetric imaging system: comparison with film radiography in detecting incipient proximal caries. *Oral surgery, oral medicine, oral pathology, oral radiology, and endodontics*. 2007 Sep;104(3):412-6.
7. Haiter-Neto F, Wenzel A, Gotfredsen E. Diagnostic accuracy of cone beam computed tomography scans compared with intraoral image modalities for detection of caries lesions. *Dento maxillo facial radiology*. 2008 Jan;37(1):18-22.
8. Tyndall DA, Rathore S. Cone-beam CT diagnostic applications: caries, periodontal bone assessment, and endodontic applications. *Dental clinics of North America*. 2008 Oct;52(4):825-41, vii.
9. Young SM, Lee JT, Hodges RJ, Chang TL, Elashoff DA, White SC. A comparative study of high-resolution cone beam computed tomography and charge-coupled device sensors for detecting caries. *Dento maxillo facial radiology*. 2009 Oct;38(7):445-51.
10. Senel B, Kamburoglu K, Ucok O, Yuksel SP, Ozen T, Avsever H. Diagnostic accuracy of different imaging modalities in detection of proximal caries. *Dento maxillo facial radiology*. 2010 Dec;39(8):501-11.
11. Qu X, Li G, Zhang Z, Ma X. Detection accuracy of in vitro approximal caries by cone beam computed tomography images. *Eur J Radiol*. 2011 Aug;79(2):e24-7.
12. Kayipmaz S, Sezgin OS, Saricaoglu ST, Can G. An in vitro comparison of diagnostic abilities of conventional radiography, storage phosphor, and cone beam computed tomography to determine occlusal and approximal caries. *Eur J Radiol*. 2011 Nov;80(2):478-82.

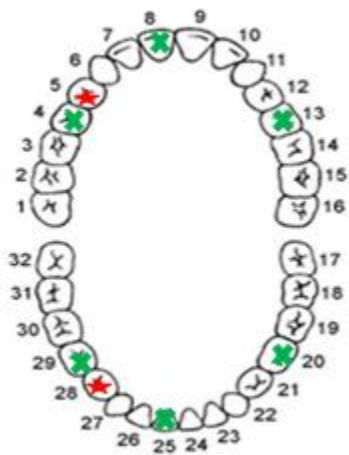
13. Charuakkra A, Prapayasatok S, Janhom A, Pongsiriwet S, Verochana K, Mahasantipiya P. Diagnostic performance of cone-beam computed tomography on detection of mechanically-created artificial secondary caries. *Imaging science in dentistry*. 2011 Dec;41(4):143-50.
14. Wenzel A, Hirsch E, Christensen J, Matzen LH, Scaf G, Frydenberg M. Detection of cavitated approximal surfaces using cone beam CT and intraoral receptors. *Dento maxillo facial radiology*. 2013;42(1):39458105.
15. Sansare K, Singh D, Sontakke S, Karjodkar F, Saxena V, Frydenberg M, et al. Should Cavitation in Proximal Surfaces Be Reported in Cone Beam Computed Tomography Examination? *Caries research*. 2014 Jan 29;48(3):208-13.
16. Welander U, Nummikoski P, Tronje G, McDavid WD, Legrell PE, Langlais RP. Standard forms of dentition and mandible for applications in rotational panoramic radiography. *Dento maxillo facial radiology*. 1989 May;18(2):60-7.

APPENDIX A

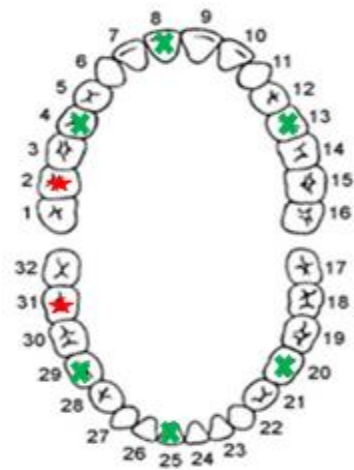
Configurations show the location (inter and intra arch) of High Density Objects (HDO).

✱ Control cylinder
★ Restoration

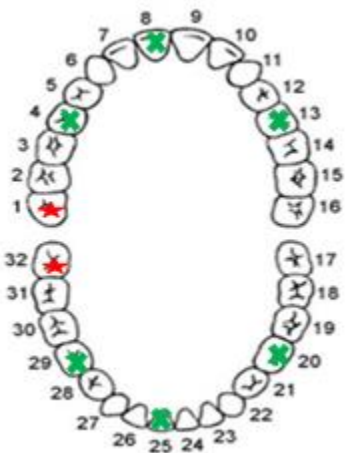
Configuration 1



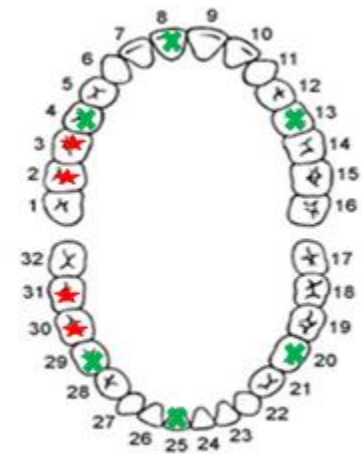
Configuration 2



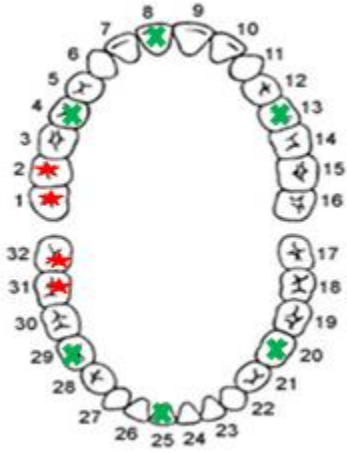
Configuration 3



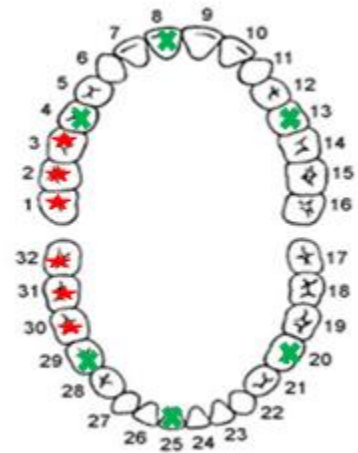
Configuration 5



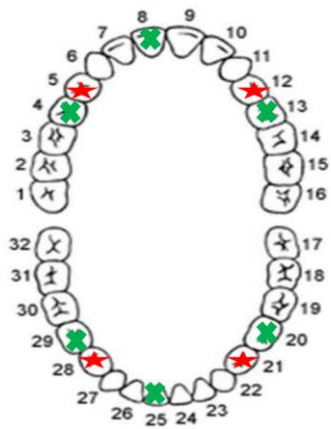
Configuration 6



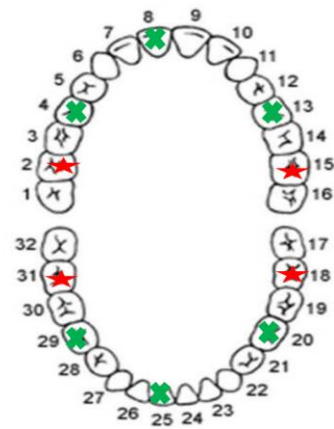
Configuration 9



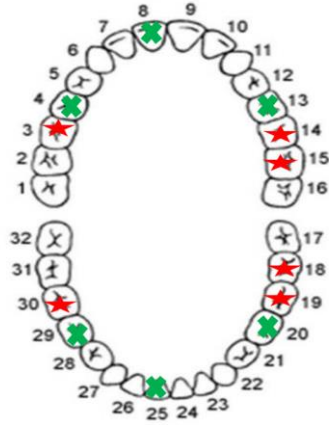
Configuration 12



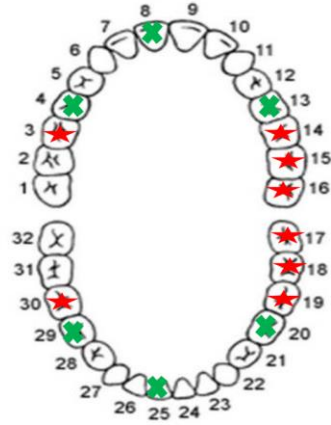
Configuration 13



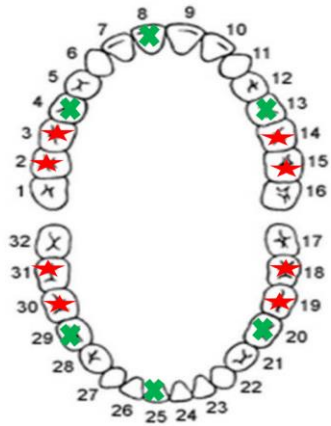
Configuration 15



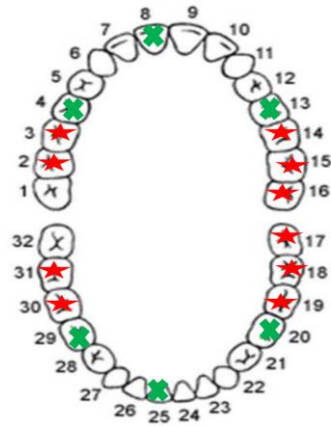
Configuration 16



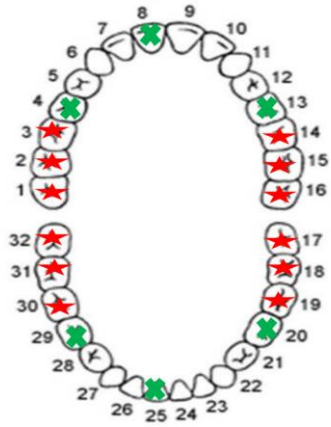
Configuration 18



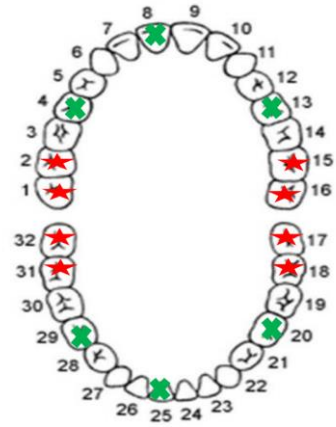
Configuration 19



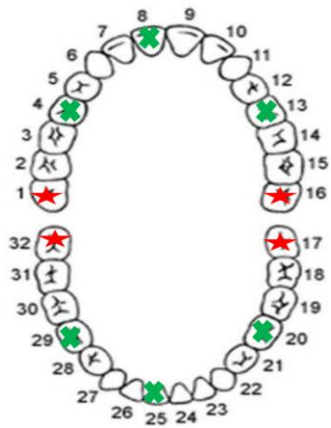
Configuration 21



Configuration 24



Configuration 25



CURRICULUM VITAE

Name: Mitali Binani
Address: 642 S. 2nd Street, Apt T304,
Louisville,
KY 40202

DOB: December 13, 1987

Education and Training:

- Bachelor of Dental Surgery (B.D.S)
Nair Hospital Dental College
2006 – 2011
- DMD (Batch of 2016)
University of Louisville, School of Dentistry
2014 -till date

Poster and Paper presentation:

- Poster: The Effect of Metallic Restoration Artifacts on Maxillofacial CBCT images.
2013
Guided by: Farman AG, Scarfe WC, Department of Surgical/Hospital Dentistry, University of Louisville School of Dentistry
Research!Louisville, 2013
- Paper Presentation: Dawn of Digital Dentistry
2011
Guided by: Dr. Aarti Wadkar, Associate Professor, Department of Prosthodontics, Nair Hospital Dental College
Scientific Rendezvous, Nair Hospital Dental College, 2010-2011